Dynamic seasonal energy management of borehole thermal energy storage and smart heat pump synergies in fossil-free, ultra-efficient buildings

Applied Energy 406 (2026) 127261

Contents lists available at ScienceDirect

Applied Energy

journal homepage: www.elsevier.com/locate/apenergy

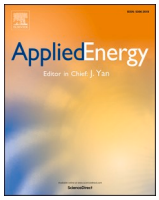

Dynamic seasonal energy management of borehole thermal energy storage and smart heat pump synergies in fossil-free, ultra-efficient buildings

Amirmohammad Behzadi [a,*], Taha Arghand [b], Christophe Duwig [c], Hailong Li [d], Sasan Sadrizadeh [a,d]

[a] Department of Civil and Architectural Engineering, KTH Royal Institute of Technology, Stockholm, Sweden
[b] Department of Architecture and Civil Engineering, Chalmers University of Technology, Gothenburg, Sweden
[c] Climate Action Centre & Department of Chemical Engineering, KTH Royal Institute of Technology, Stockholm, Sweden
[d] School of Business, Society and Engineering, Mälardalen University, Västerås, Sweden

HIGHLIGHTS

- A novel heat pump integration method is introduced in a real low-carbon building.
- The new system extracts 27 % more ground heat via a better thermal balanced layout.
- Initial investment rises 11 %, while NPV increases by 20 % over the 20-year horizon.
- Annual heating cost falls by 29 % using a dynamic, seasonally adaptive controller.
- CO_2 emissions drop, reaching 22.6 kg/MWh via a smart hybrid system operation.

ARTICLE INFO

Keywords:
Ground source heat pump
Low-carbon buildings
Borehole TES
Advanced control strategies
Thermal energy management

ABSTRACT

Thermal energy demand in buildings represents one of the largest contributors to global energy use and CO_2 emissions. Advanced thermal energy systems, including borehole thermal energy storage (BTES) integrated with highly intelligent air handling units, offer promising solutions to reduce emissions while ensuring affordable and reliable comfort. This study examines a state-of-the-art commercial building in Uppsala, Sweden, that already employs a fossil-free and highly efficient BTES–district heating configuration. Although this system is well-designed and operates intelligently, it still has important limitations, including underutilization of borehole potential, limited thermodynamic efficiency from direct-use exchange, and a lack of flexibility under varying energy tariffs. Therefore, this work aims to make an already smart and efficient system even smarter by integrating a ground source heat pump with adaptive seasonal energy management. A comparative benchmarking analysis is carried out using validated TRNSYS simulations and real operational data to evaluate performance, economic viability, and environmental outcomes. The results show that integrating a clever heat pump system enhances the annual heat extraction from the ground by approximately 27 %, resulting in a 29 % decrease in overall heating costs, and improves long-term savings by around 20 %, despite an 11 % rise in upfront investment. Environmentally, the enhanced system substantially reduces CO_2 emissions, cutting the annual impact by more than 90 % compared to the current configuration, aligning with the Swedish zero-emission targets. However, the operational cost savings strongly depend on peak heat (power) costs, which are expected to rise under policymakers' frameworks. This indicates that the long-term viability of adding heat pumps in Sweden is shaped not only by technical performance and CO_2 savings but also by evolving local energy price structures. Yet, the considerable CO_2 savings helped by Sweden's green electricity mix and the opportunity to enjoy hourly spot-price variability through advanced controllers make heat pump integration a compelling option for future-proofing ultra-efficient buildings.

* Corresponding author.
E-mail address: abehzadi@kth.se (A. Behzadi).

https://doi.org/10.1016/j.apenergy.2025.127261
Received 23 May 2025; Received in revised form 28 November 2025; Accepted 12 December 2025
Available online 22 December 2025

1. Introduction

In alignment with UN Sustainable Development Goal 7, which advocates for affordable and clean energy, it is essential to address heating demand in cold climates, particularly in northern Europe and Scandinavia, where it constitutes approximately 60–70 % of total building operational energy use [1,2]. As buildings transition to low-energy or nearly zero-energy norms, the imperative to fulfill heating demands efficiently while reducing reliance on fossil-fuel-based district heating systems intensifies [3]. This necessitates designing and implementing intelligent heating, ventilation, and air conditioning (HVAC) systems that adjust to variable loads, incorporate more renewable energy sources, and reduce peak energy use and operational expenses [4].

Ground resources in cold climates offer significant potential for renewable energy, as they maintain stable and predictable temperatures, particularly at depths exceeding 200 m. This characteristic makes them an effective medium for both passive and active thermal energy exchange. In Sweden, the natural temperature stability allows the ground to function as a renewable source for both heating and cooling [5]. Drilling boreholes and installing borehole thermal energy storage systems enable buildings to utilize stored energy seasonally, allowing for the accumulation of excess heat in summer and its extraction during winter [6]. Numerous studies have shown the potential and effectiveness of borehole thermal energy storage. For instance, Shah et al. [7] created a validated TRNSYS model to evaluate a seasonal solar thermal energy storage system utilizing borehole storage in six cold-climate locations. Their findings indicated that the system may satisfy more than 90 % of annual room heating needs while preserving stable ground temperatures through solar charging. Giordano and Raymond [8] developed and modeled a borehole thermal energy storage system in subarctic Kuujjuaq, Canada, to evaluate its viability under extreme cold temperatures. They determined that these systems can recover over 60 % heat by the third year and substantially decrease diesel use. Ekmekci et al. [2] modeled a borehole thermal energy storage system for residential heating in Sweden. By the fifth year, they determined the system could fulfill all heating demands using stored energy, providing practically costless and emission-free heating. Fiorentini et al. [9] developed an advanced system utilizing borehole thermal energy storage, achieving emissions reductions of up to 43.7 % with minimal additional costs, thereby enhancing the efficiency and climate responsiveness of BTES systems. Saitoh and Yamaguchi [10] introduced a seasonal thermal energy storage system that utilizes 100-m-deep boreholes to heat and cool high-story buildings. The simulations demonstrated that the system efficiently reuses waste heat from summer and cold from winter, providing energy efficiency and potential reductions in CO_2 emissions in urban environments.

Although passive systems have demonstrated effectiveness, their capacity to collect heat is inherently constrained by temperature differentials. Heat pumps, particularly water-to-water ground source heat pumps (GSHPs), exhibit a significant advantage when combined with borehole thermal energy storage, due to their elevated coefficient of performance (COP) [11,12]. These systems generally attain COP values ranging from 3 to 5, indicating that each unit of electricity utilized can provide three or more heat units, thus demonstrating high energy efficiency. Huo et al. [13] proposed a borehole-driven heating system integrated with a ground-source heat pump to meet the district's demand. The study concluded that employing an equivalent borehole transfer function preserves high geothermal heat pump efficiency by ensuring stable ground temperatures. Naranjo-Mendoza et al. [14] investigated a solar-driven GSHP utilizing boreholes for seasonal heat storage in a residential building. The system effectively addressed all heating demands and adjusted the ground thermal imbalance; however, enhancements in control strategies were suggested to optimize performance. Fiorentini et al. [15] modeled a borehole thermal energy storage system integrated with a heat pump interacting with a district heating network. They demonstrated that integrating heat pumps with borehole thermal energy storage can lead to emissions reductions of up to 43 % compared to a traditional system based on the air-source heat pump standalone. Naldi and Zanchini [16] investigated a borehole-driven heating and cooling system combined with heat pump systems under various design conditions. The study demonstrated that extending the borehole length and employing inverter-driven heat pumps can significantly improve system efficiency by up to 30 % for heating and 40 % for cooling. Zhu et al. [17] studied the feasibility of integrating a heat pump system with borehole thermal energy storage for a residential building in Xi'an. They found that coupling with a heat storage tank reduced heating costs by 13 % and improved system COP by over 10 %, making it a more economically favorable solution than a standalone borehole system.

Recent comparative studies have explored the trade-offs between configurations, specifically systems utilizing boreholes combined with district heating, and those models combined with ground-source heat pumps [18–20]. Minimizing dependence on DH is increasingly critical due to fluctuating and seasonally variable tariffs, especially with the implementation of peak power-based pricing structures that substantially impact operational expenses for commercial buildings [21]. In this context, GSHPs present a viable approach to redirecting heating demand from the DH network, especially when integrated with boreholes, facilitating enhanced utilization of on-site renewable thermal energy [22–24]. Hemmatabady et al. [25] assessed the potential of incorporating a heat pump system into a fourth-generation district heating system, demonstrating that the borehole thermal energy storage system integrated with heat pumps achieves higher efficiency and lower heating and cooling costs than the borehole-only model. Fiorentini and Baldini [26] developed a control model to optimize the operation of a heat pump-driven borehole thermal energy storage system. The study concluded that seasonal variation in electricity carbon intensity significantly influences optimal operating strategies, potentially reducing CO_2 emissions by up to 20 % compared to a model based solely on borehole thermal energy storage. This effect is more significant in countries exhibiting higher or more variable electricity carbon intensity than in Sweden. Arghand et al. [27] conducted an analysis on the integration of direct ground cooling with ground-source heat pumps and district heating systems in office buildings in Sweden. Their research indicated that the borehole-driven system, when interacting with the district heating network, generally results in reduced electricity usage and lower investment and lifecycle costs. Conversely, when ground loads are effectively balanced, the borehole + district heating + heat pump system demonstrates lower total operational costs (heating+electricity). Li et al. [20] compared 5th-generation district heating and cooling systems, which are defined by low-temperature distribution utilizing borehole thermal energy storage with and without the integration of heat pumps. According to their results, the borehole-only system presents reduced investment costs. However, interpreting investment costs is context-dependent, as some infrastructure components, such as the district heating network, are typically owned by utilities rather than the end-user, which complicates direct comparisons of capital costs.

Recent developments in low-carbon Heating, ventilation, and air conditioning (HVAC) systems have presented several promising alternatives, including solar-assisted ground source heat pumps, fifth-generation district heating and cooling, and hybrid solutions that integrate thermal storage with renewable electricity. Solar-assisted ground source heat pump systems enhance self-sufficiency and mitigate seasonal imbalances; however, they typically necessitate substantial collector area, involve elevated capital costs, and add design complexity [28,29]. Similarly, 5th-generation district heating and cooling networks offer significant flexibility and overall efficiency, but they depend on centralized infrastructure and coordinated energy planning [30].

Despite extensive research on borehole thermal energy storage and ground source heat pump systems, the majority of studies tend to concentrate on idealized simulations or analyze these systems in isolation. This often results in the oversight of essential real-world factors,

including interactions with existing district heating networks, the impact of tariff structures and carbon intensity on operational strategies, long-term seasonal imbalances in ground temperature, and the practical challenges associated with the implementation of advanced control systems within buildings and utility frameworks. Limited critical assessment exists regarding the extent to which existing systems exploit the renewable potential of boreholes, as well as the performance enhancements achieved through the transition from passive boreholes to active heat pump integration. Furthermore, comparative analyses are limited and based on simple or idealized system configurations. Specifically, research is lacking that compares systems integrating borehole thermal energy storage with district heating to hybrid configurations incorporating ground-source heat pumps, particularly in evaluating techno-economic performance, operational behavior in real-world scenarios, and long-term environmental consequences. Although numerous studies investigate the control and performance of borehole and heat pump systems, there is a lack of research focusing on control-oriented factors, such as seasonal borehole charging strategies and dynamic heat pump scheduling, that concern key performance outcomes, including payback period and CO_2 intensity, within a comprehensive and practically applicable framework.

In order to fill these research gaps, this study examines a smart, ultra-efficient commercial building in Uppsala, Sweden, which utilizes passive borehole thermal energy storage in conjunction with the district heating network [31]. Initially developed by Skanska within its Deep Green Cooling framework, the system is both fossil-free and innovative; however, it exhibits operational limitations, such as:

- The utilization of borehole heat extraction is limited by its dependence on the air handling unit's preheating coils, which operate solely at low outdoor air temperatures, thereby restricting the effective use of ground heat resources.
- Although mechanically straightforward, the current direct heat exchange configuration exhibits lower conversion efficiency than a heat pump system in raising low-temperature ground heat to usable levels for space heating with minimal electricity use at an acceptable COP.
- A seasonal recharge strategy for the boreholes is lacking, which may result in thermal imbalance and a progressive decline in performance over time.
- District heating tariffs are fixed seasonally, while electricity prices vary hourly in Sweden; this flexibility remains untapped for cost optimization, load shifting, and advanced control.

To provide a structured overview of the research context, Fig. 1 summarizes the progression from the identified problem to the contributions of this study. This research seeks to address the following research questions:

- What is the extent of additional thermal potential that may be harnessed from the boreholes through GSHP integration?
- Can a seasonal borehole charging technique sustain long-term thermal equilibrium while diminishing reliance on district heating?
- What are the long-term economic and carbon performance trade-offs associated with upgrading an already high-performing, low-carbon building through smart component integration and seasonal energy management?

The remainder of this paper is structured as follows: Section 2 presents the methodology, including a description of the case study, system configurations, model development, and stability analysis. Section 3 reports the results of the comparative performance assessment in terms of energy, economic, and environmental outcomes. Finally, Section 4 presents the key findings and implications, as well as the study's limitations.

2. Method

The performance of two smart heating and cooling system configurations in a commercial building in Uppsala, Sweden, is assessed and

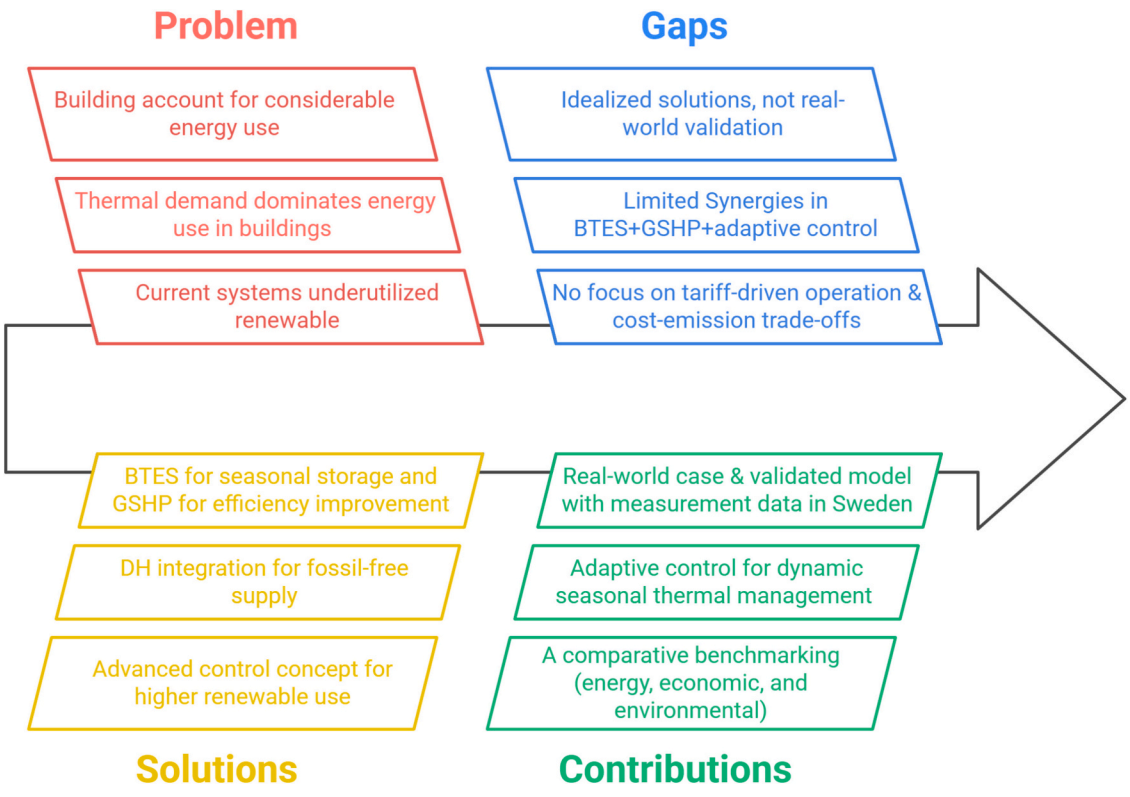

Fig. 1. Conceptual framework of the present work, highlighting the problem, existing solutions, identified research gaps, and the contributions of this work.

compared in this study using a case-study methodology. The methodology consists of three key parts: (1) a description of the case study building and its location-specific parameters, (2) a comprehensive presentation of the existing smart HVAC system alongside the proposed system integrated with a downsized heat pump, and (3) the development of a dynamic model to simulate and evaluate the performance of both systems from various perspectives under realistic boundary conditions. This section provides a detailed description of each component.

2.1. Case study

2.1.1. Building and climate

This research's case study is the property Juvelen, a recently constructed commercial building located adjacent to the main train station in the historic city of Uppsala, Sweden (see Fig. 2). Juvelen is acknowledged as one of the most sustainable structures in the Nordic region, exemplifying the convergence of creative architecture and superior environmental design. Juvelen is a six-story building that includes offices and a restaurant. It has a total area of 10,000 m^2. Developed by Utopia Arkitekter and designed by Skanska, the building attained LEED Platinum certification and is designated as a "Dark Green" project within Skanska's internal sustainability assessment framework, finalized in 2019 [31].

Juvelen includes Skanska's patented Deep Green Cooling technology, a passive thermal system that removes the necessity for traditional chillers or heat pumps [32]. The system employs deep borehole thermal energy storage to leverage the earth's stable temperatures, facilitating direct cooling of the building via a closed-loop fluid circuit. Deep Green Cooling differs from existing systems that utilize electrically driven compressors by circulating a coolant, usually water or a water-glycol mixture, where the ground temperature consistently remains low throughout the year (typically 8–12 °C in Sweden). This low-grade thermal energy is adequate for high-temperature cooling applications, including chilled beams and post-cooling coils, without mechanical compression or active refrigeration. The system demonstrates full compatibility with smart HVAC design and achieves notable energy performance up to 5–6 times more efficiently than mechanical cooling with a self-sufficient and climate-resilience method. This leads to considerable decreases in electricity usage, especially in summer, and facilitates net-zero or fossil-free building operations. The required data needed to model the proposed building, including set points, heat transfer coefficient values, window/wall ratio, and glazing details, can be found in Table A1 in the Appendix.

Fig. 2. The studied commercial building in Uppsala, Sweden [31].

Uppsala exhibits a cold temperate climate (Dfb as per the Köppen classification), marked by extended, cold winters and mild to warm summers [33]. Fig. 3 presents Uppsala's monthly outdoor temperature fluctuations derived from historical data. Fig. 2 illustrates that monthly mean temperatures vary from approximately −5 °C during winter to 17–18 °C in summer, with recorded extremes falling below −10 °C and exceeding 25 °C. The undisturbed ground temperature at borehole depth typically aligns with the annual average outdoor temperature, approximately 6.5 °C in Uppsala. The region's low and stable ground temperature renders it ideal for direct ground cooling, facilitating passive thermal solutions that do not require mechanical chillers.

2.1.2. Energy system

Fig. 4 depicts the proposed smart HVAC system operating in Juvelen as built, originally integrating boreholes with the district heating network to meet the heating and cooling needs of the building. The system connects to three air handling units: two for office spaces and one specifically for a restaurant. During winter, heat is extracted from the boreholes and transferred through a free heating heat exchanger to preheat the ventilation air using the preheating coils, which PID controllers regulate [31]. When extra heating is necessary for indoor comfort levels, post-heating coils and radiators utilize heat from the district heating network. The district heating network also provides domestic hot water via a heat exchanger.

The system functions in passive cooling mode during the summer months. The boreholes operate as a heat sink, absorbing surplus thermal energy from the building through a free cooling heat exchanger. The cooled water exiting the boreholes with moderate temperatures (~16 °C) from the ground is distributed to either the post-cooling coils in the air handling units or the active chilled beams in the office zones. Chilled beams are high-temperature cooling devices that operate efficiently and moderately, ensuring compatibility with direct ground cooling and negating the necessity for mechanical chillers. The cooling reserve is a room where heat-generating components, such as computers, are located. This hybrid system enables the building to extract heat from the ground in winter and reject heat into the boreholes in summer, thereby establishing a seasonally balanced storage loop. Integrating passive ground-based heating and cooling with the dependable support of the district heating network guarantees year-round comfort, operational reliability, and reduced electricity usage, all achieved without the use of chillers or active refrigeration systems.

The ventilation system includes a recovery heat exchanger (offices), a run-around heat exchanger (restaurant), supply and exhaust fans, and intelligent controls that oversee supply air temperature, indoor

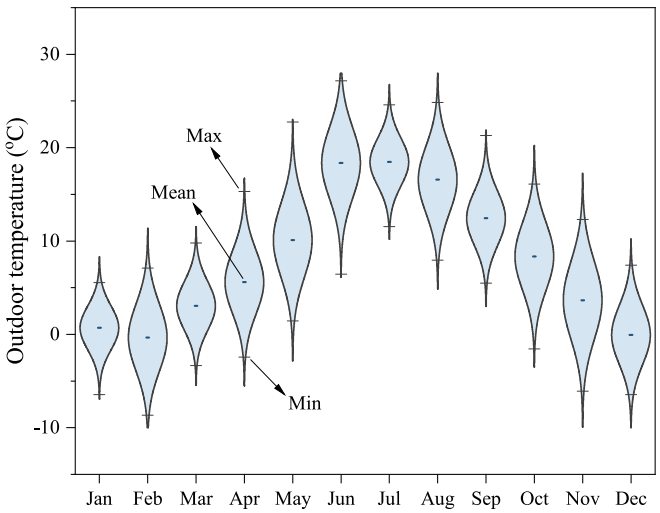

Fig. 3. The monthly changes in outdoor temperature in Uppsala, Sweden [34].

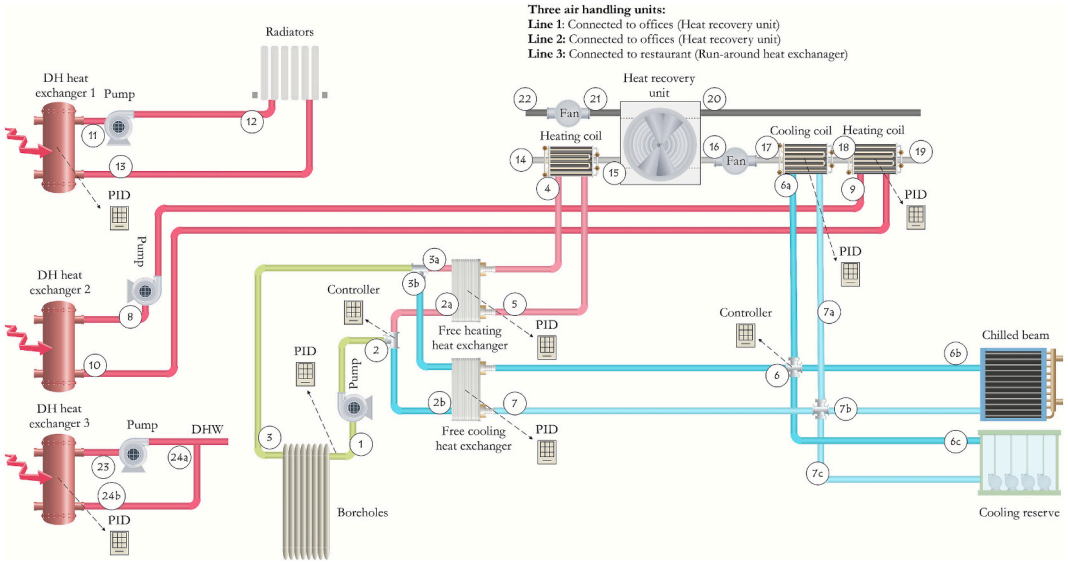

Fig. 4. The schematic representation of the proposed smart HVAC system operating in Juvelen, based on boreholes interacting with the DH network [35].

setpoints, and comfort thresholds. The run-around heat exchanger is used in the air handling unit connected to the restaurant to avoid mixing undesirable odors, oils, or smoke from the restaurant's exhaust air with the inlet fresh air. The proposed smart system also features various controllers, including ON/OFF and PID, to dynamically regulate fluid routing and airflow, ensuring that the comfort and temperature settings of different components are met. The controllers consistently react to real-time inputs, including indoor temperature, outdoor conditions, the status of HVAC components, and occupancy schedules, enabling the system to operate efficiently while ensuring thermal comfort. This adaptive, demand-responsive control strategy plays a key role in the proposed smart HVAC system.

After examining the existing system configuration in detail, it was observed that, although the current system already delivers excellent performance, three structural limitations remain (see Fig. 5).

The first limitation is that the borehole potential is underutilized in the current system. Currently, the boreholes are connected only to the preheating coils of the air handling units. During transitional seasons, when outdoor air is sometimes warmer than the borehole water, the preheating bypasses entirely, leaving much of the borehole capacity unused. The second problem is the Limited thermodynamic potential. In the current setup, the boreholes are used in a simple direct-exchange configuration, where the efficiency is restrained by the temperature difference between the two fluids. By contrast, introducing a water-to-water ground-source heat pump would significantly raise efficiency. With a COP generally above 4, it upgrades low-grade geothermal energy

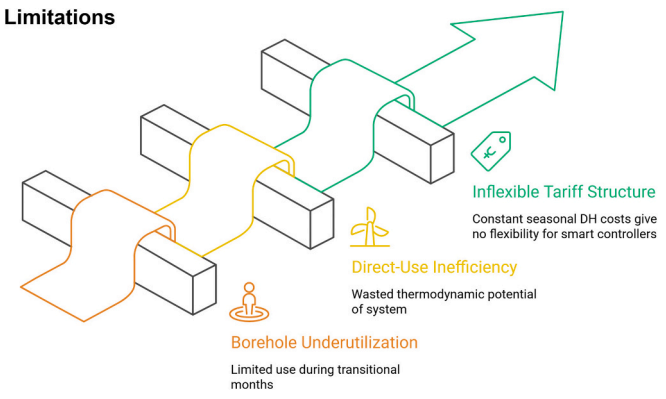

Fig. 5. Limitations of the existing borehole–DH system.

to heating supply temperatures with minimal electricity use, greatly improving conversion efficiency. The last but not least important limitation is the Lack of operational flexibility. District heating prices are typically fixed on a seasonal basis, whereas electricity prices in Sweden fluctuate on an hourly basis. By integrating a GSHP, the system can take advantage of these fluctuations, operating more during low-price hours and less during peak times. This creates opportunities for load shifting, peak shaving, and dynamic cost optimization, particularly under model predictive control strategies. Recognizing these limitations, the study proposes an alternative system configuration that integrates a ground source heat pump with borehole thermal energy storage and a seasonal charging strategy, aiming to overcome inefficiencies, enhance flexibility, and unlock the full potential of the existing configuration.

2.2. The alternative energy system

Fig. 6 illustrates the improved system configuration, wherein the groundwater-filled boreholes are coupled with a ground source heat pump exclusively (two heat pumps with a capacity of 40 kW each) for heating. The primary modification occurs within the heating loop: heat extracted from the boreholes is now directed to the heat pump's evaporator rather than the preheating coils, thereby enhancing the low-temperature energy to a usable level. The condenser output supplies the building's radiator circuit, thereby significantly decreasing the building's dependence on the district heating network for space heating. This alternative configuration, commonly employed in Sweden, exemplifies a hybrid setup in which the ground-source heat pump is integrated with district heating, particularly during peak demand periods or when the heat pump's efficiency is compromised. The system facilitates more effective and consistent heat extraction by decoupling borehole use from direct air preheating, thereby operating independently of fluctuations in outdoor air temperature.

This study assesses the thermal behavior of the borehole TES system over a one-year operational period; however, the long-term sustainability of these systems is significantly affected by the evolution of ground temperature over multiple years. Numerous studies indicate that imbalanced annual heat extraction, without adequate seasonal compensation, may lead to a gradual decrease in borehole temperature. This decline subsequently diminishes heat pump efficiency and elevates electricity usage [14,36,37]. In order to achieve a long-term thermal balance in boreholes, a charging heat exchanger is added to the system to transfer heat to the ground during periods of low demand, particularly in September. This component is essential for compensating for the

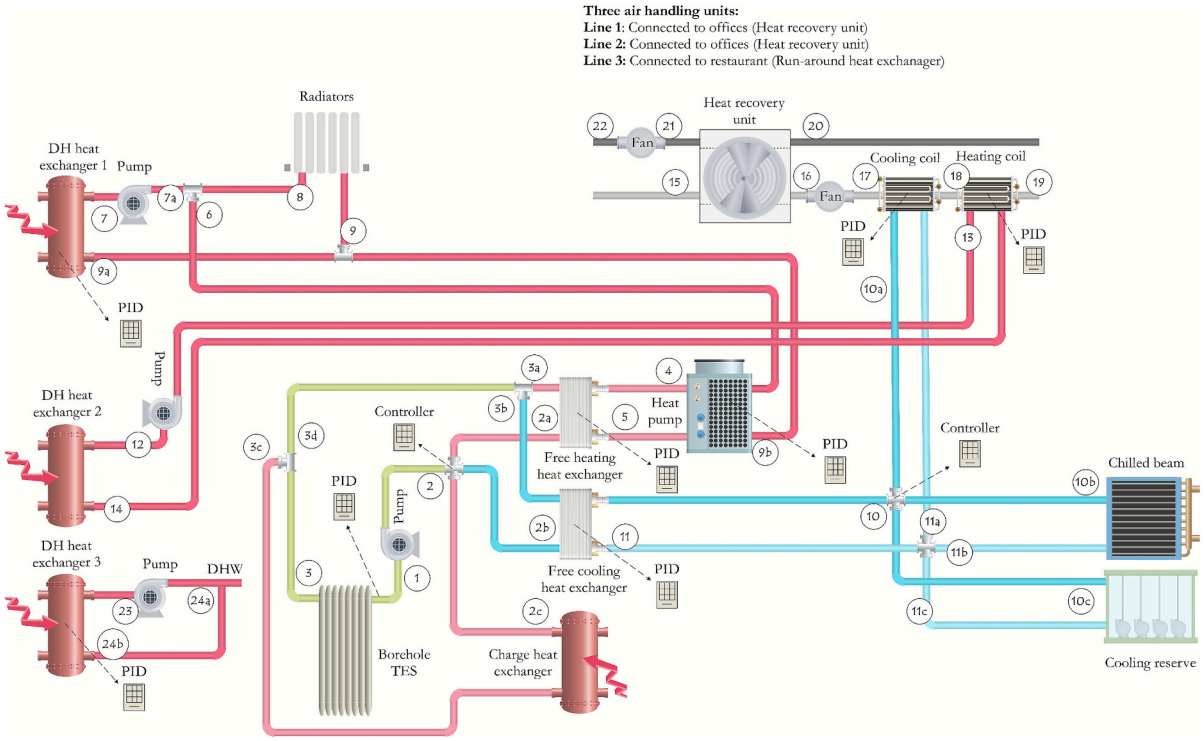

Fig. 6. The schematic representation of the alternative system based on the ground source heat pump supplemented by the DH [35].

substantial heat loss from the boreholes during winter through the ground source heat pump. Continued extraction without recharging over multiple seasons may gradually decline borehole temperatures, thereby diminishing heat pump efficiency and risking system sustainability. The charging process is regulated by a PID controller that monitors the average ground temperature and initiates heat injection when it drops below a specified reference, typically set to return the borehole temperature to its baseline value from the start of the year. The heat is obtained from the district heating network, which provides lower seasonal tariffs in September, thereby serving as a cost-effective method for rebalancing the thermal reservoir while minimizing significant impacts on operational costs. The new heating strategy does not alter the cooling operation, which continues to utilize boreholes for passive cooling via a free cooling heat exchanger linked to active chilled beams and cooling coils, especially in office areas.

2.3. Operating strategy for adaptive seasonal thermal management

The suggested alternative system operates under an adaptive control strategy designed to maintain seasonal thermal balance while minimizing operating costs. The heat pumps are governed through a hierarchical logic: during periods of low to moderate space-heating demand, a single 40 kW unit operates at full load to preserve high COP, and the second unit is activated only when the radiator demand exceeds the capacity of one unit. The radiator supply temperature is regulated by a PID controller, which adjusts the heat pump's output to track the indoor thermal setpoints.

The borehole field functions as a seasonal thermal battery, storing heat during summer and releasing it during winter. This behavior is achieved through a dedicated seasonal management scheme and the integration of smart components. The system is also equipped with a PID-regulated charging strategy, which was applied in September. During this period, the controller monitors the average borehole temperature and activates the charging heat exchanger when the measured value falls below the January reference level. Heat from the district-heating network is injected until the baseline temperature is restored. This process ensures long-term thermal stability, maintains favorable evaporator inlet conditions, and prevents COP degradation during peak winter operation.

The overall operating strategy, therefore, couples short-term load-responsive control with long-term seasonal thermal balancing. This coordinated interaction among the heat pumps, borehole TES, and district-heating network delivers the adaptive behavior highlighted in the contribution framework (Fig. 1) and forms a central component of the proposed smart seasonal energy management concept.

2.4. System simulation

This study built a detailed simulation model utilizing TRNSYS 18 to assess and compare the performance of two smart HVAC system designs under actual climatic and operational conditions. The model integrates advanced component-level dynamics and has been calibrated with high-resolution data obtained from the building management system (Tekla) supplied by Juvelen's property owner, Vasakronan AB. This data contains hourly operational metrics of HVAC subsystems and building demand profiles throughout the year. Each component is represented by a designated TRNSYS type, with its behavior dictated by thermodynamic, fluid dynamics, and control system equations as outlined in the TRNSYS component manuals (see Table 1). According to the table, in boreholes, the simulation incorporates convective heat transfer within the U-tube and conduction through the adjacent ground, employing a hybrid solution methodology that integrates 1) a global solution for long-term ground temperature dynamics, 2) a local solution for thermal interactions surrounding individual boreholes, and 3) a steady-state flux solution for constant thermal loads. The ground temperature field is resolved by finite difference techniques, employing a superposition method for combination. This method enables the precise modeling of both short-term variations and long-term seasonal influences. The model incorporates the thermal resistance of the borehole grout, pipe materials, and the properties of the heat carrier fluid, all of which are determined from field data and manufacturer specifications. Type 827 utilizes catalog-derived performance data to evaluate heating capacity

Table 1
The TRNSYS component types and their corresponding descriptions.

Type	Description
577	It mimics vertical ground heat exchangers, thermally interacting with the surrounding soil. This component denotes a U-tube or concentric pipe ground heat exchanger, wherein a heat transfer fluid (specifically, a 30/70 Ethylene Glycol/Water mixture) circulates through a series of vertical boreholes, extracting heat from the ground in winter or rejecting heat back into the ground in summer. The boreholes are evenly distributed within a cylindrical soil volume, comprising 25 vertical U-tube boreholes, each 250 m in depth and separated by 6 m.
827	It models a two-stage, water-to-water heat pump utilizing performance maps. This component illustrates the functionality of the NIBE F1345 heat pump unit, tailored for commercial-scale applications (see Table A3 in the Appendix).
667	The energy wheel in this system, modeled with TRNSYS Type 667, functions as a rotary heat exchanger that recovers both sensible and latent heat from exhaust air to precondition incoming fresh air. This component is essential for reducing ventilation-related heating and cooling loads, particularly in cold climates such as Sweden, where outdoor air temperatures drop significantly during the winter months.
753	It simulates a hot water-based air heating process through a bypass fraction method. Warm water circulates through the coil, allowing a portion of the incoming air to reach thermal equilibrium with the average fluid temperature within the coil. In contrast, the rest of the air bypasses the coil without alteration. The heat transfer to the air stream is determined using the bypass fraction and the log-mean temperature difference (LMTD) method.
508	The cooling coil is represented using Type 508, which employs a bypass fraction method to simulate air cooling and dehumidification. A specified air segment bypasses the coil, while the remainder is presumed to be cooled to the average fluid temperature and exits the coil under saturated conditions, indicating the maximum potential for latent and sensible cooling. The component operates in two modes: uncontrolled mode, which maximizes heat and moisture removal based on inlet conditions, and controlled operation, where a portion of the fluid or air stream is bypassed to maintain outlet temperatures below a specified maximum threshold.
91	It models a steady-state, design-independent liquid-to-liquid heat exchanger. This component facilitates heat exchange between two fluid streams, specifically the borehole circuit and the internal building loop, in contrast to air coils. The model employs a fixed effectiveness method, whereby the outlet temperatures are established based on the assumed effectiveness and the minimum heat capacity rate of the two streams.
22	The iterative feedback controller, modeled with Type 22, maintains a target value for a designated system variable by continuously adjusting the input until the desired output is achieved. This controller is particularly beneficial in HVAC systems, where interdependent variables and nonlinear behaviors complicate simple control logic.
23	The proportional–integral–derivative (PID) controller, utilized through TRNSYS Type 23, is essential for regulating dynamic system responses, particularly in components that exhibit time-dependent behavior, such as pumps, heat pumps, and valves.
106	The thermostat controller is a straightforward yet efficient on/off control system that operates according to specified temperature thresholds. This mechanism activates or deactivates components, including heat pumps or valves, based on whether the measured temperature surpasses or drops below the specified upper and lower setpoints. This controller employs a hysteresis band to mitigate frequent cycling, thereby enhancing the longevity and efficiency of mechanical systems. It enhances the dynamic control offered by Type 23 and is especially beneficial for threshold-based system switching.
744	It simulates a variable-speed fan or blower functioning against a predefined pressure drop. The component calculates electric power consumption and airflow delivery based on the defined fan curve, which is generally characterized by a quadratic relationship between airflow and pressure increase.
110	The circulation pumps on the fluid side, which transport water through boreholes, heat exchangers, and coils, are modeled with TRNSYS Type 110. This component represents a variable-speed pump that calculates the power consumption required to circulate a designated fluid at a specified mass flow rate against a specified pressure drop.

and power input under various operating conditions. This encompasses fluctuations in brine inlet temperature, heating supply temperature, and mass flow rates, facilitating dynamic system simulation throughout the year. The model employs non-dimensional performance maps that correlate the heat pump's output with the inlet brine temperature (from borehole thermal energy storage) and the outlet setpoint temperatures (to radiators). The heat pump functions as a water-to-water system, with its evaporator linked to a borehole loop that circulates a 30/70 ethylene glycol–water solution. The fluid temperature may occasionally drop below 0 °C in winter; however, the system avoids frost-related efficiency losses due to the absence of air-side heat exchange. Consequently, defrosting cycles were excluded from the modeling in this study.

The Appendix provides additional details on the system design and input parameters required for completing the simulation. Included are airflow schedules, thermal and physical properties, heat pump specifications, and occupancy profiles (refer to Tables A1–A2). It also includes the TRNSYS Studio schematics of the modeled system configurations (Fig. A1).

2.5. Mathematical modeling and stability of the alternative configuration

To ensure a thorough evaluation of the proposed alternative system (Fig. 4), it is essential to augment the schematic representation with a comprehensive mathematical formulation and a stability study. TRNSYS offers a modular framework in which each component is represented by specific Types coded in Fortran and validated/verified by the Solar Energy Laboratory at the University of Wisconsin–Madison. This section outlines the fundamental thermodynamic relations of the ground source heat pump, the energy balance of the condenser-evaporator loop, the control algorithms for space heating and seasonal borehole charging, and the stability criteria.

This study regulates heat pump operation using a PID controller (Type 23), prioritizing logic according to radiator demand and internal temperature setpoints. Type 667 is designed to replicate the function of enthalpy wheels, which facilitate heat transfer and moisture. However, in this specific application, the predominant mode is sensible heat recovery, attributed to the dry winter conditions. The model computes the outlet temperatures of both air streams using user-specified effectiveness values for sensible and latent heat transfer. The PID controller consistently evaluates the measured value (e.g., indoor temperature, supply fluid temperature) against the setpoint and modifies the control signal to reduce the error. This approach guarantees stable system control, minimizes overshoot, and enhances energy efficiency by closely aligning with thermal comfort and energy objectives. As mentioned earlier, the seasonal heat charging strategy is implemented in September to prevent long-term temperature drift and ensure the thermal sustainability of the boreholes. The control mechanism is regulated by a PID controller, which manages heat input from the DH network. The control variable is the average borehole TES temperature at time t (T_{avg} (t)). The setpoint temperature (T_{set}) is the average borehole temperature recorded on January 1 of the same year. The calculation of the temperature error is as follows:

$$e(t) = T_{ref} - T_{avg}(t) \tag{1}$$

The charging power supplied by DH is calculated by:

$$Q_{charge}(t) = K_p.e(t) + K_i \int_0^t e(\tau)\, d(\tau) - K_d.\frac{de(t)}{dt} \tag{2}$$

In this equation, K_p, K_i, and K_d are the proportional, integral, and derivative gains. The control logic operates only in September and is deactivated when the average temperature exceeds the reference temperature.

Table 2 describes the mathematical modeling of the ground-source heat pump system used in TRNSYS. The formulation includes the energy balance, the coefficient of performance, and the dependence of compressor power on critical operating factors, derived from manufacturer catalog data through interpolation. The energy balance guarantees that the heat the condenser provides to charge the radiators is equivalent to the total heat removed from the boreholes and the power supplied to the compressor. The COP expression measures the heat pump's

Table 2
Mathematical modeling of the ground source heat pump system.

Equation	Descirption
$Q_{condenser} = Q_{evaporator} + W_{compressor}$	Energy balance, indicating that the heat delivered to the condenser equals evaporator heat plus compressor power
$COP = \frac{Q_{condenser}}{W_{compressor}}$	Coefficient of Performance: ratio of useful heating output to compressor power
$W_{compressor} = f\left(T_{source,in}, T_{load,out}, \dot{m}_{source}\right)$	Compressor power input as a function of source inlet temperature, load outlet temperature, and source mass flow rate (interpolated from manufacturer catalog)

efficiency by correlating the usable heating output with the electrical input required. The relationships are integrated into the TRNSYS simulation to assess the dynamic performance and stability of the GSHP system under fluctuating operational and seasonal conditions.

The stability of the alternative configuration is assessed through the operation of the heat pump, the borehole's thermal balance, and the performance of the control system. For this, the heat pump compressor should operate within the manufacturer's specified performance parameters to prevent fluctuations in source inlet and load outlet temperatures from causing instability or inefficiency. The seasonal adaptive charging strategy for the borehole's long-term stability was implemented in September. The goal is to annually set the average ground temperature to its January baseline. Control stability is achieved via regulation of radiator supply and indoor air temperatures. It aims to minimize oscillations, reduce heat pump cycling frequency, and ensure thermal comfort. Finally, empirical corroboration is carried out by keeping the monthly COP consistently within a range of ~4.5–5 following borehole recharging, with a peak in October, which confirms that the system operates in a stable and efficient regime throughout the heating season. This framework for structured stability assessment guarantees both short-term dynamic behavior and long-term sustainability in the GSHP–borehole–DH configuration. The analysis integrates theoretical formulations, control-based mechanisms, and simulation proofs, establishing a solid basis for performing a comparative techno-economic-environmental comparison in Section 3.

2.6. Emission factors and energy pricing

Uppsala's district heating system is comprehensive and advanced, serving over 90 % of the city's buildings. The system predominantly utilizes combined heat and power plants powered by biomass and waste incineration. The national electricity grid in Sweden is increasingly powered by renewable sources, particularly hydropower, wind energy, and nuclear energy, resulting in one of the lowest carbon intensities in electricity production in Europe. For this study, the emission indices for Uppsala's electricity and heating networks (SE3) are 27 g CO_2e/kWh and 45.8 g CO_2e/kWh [38]. The overall CO_2 emissions of both systems depend on the energy source mix of the power grid and the district heating network, as they interact to meet heating and electrical demands. Simultaneously, both systems utilize boreholes as a primary source of heating and cooling, which is deemed CO_2-free. The following equation is employed to quantify the total operational CO_2 emissions:

$$CO_2\ used = Heating\ index \times (Heating\ purchased\ from\ the\ DH\ network) + Electricity\ index \times (Electrcity\ purchased\ from\ the\ grid) \quad (3)$$

In this equation, the heating and electricity indices are 45.8 gCO_2e/kWh and 27 gCO_2e/kWh, respectively. In order to further compare and normalize the environmental performance of each system, the CO_2 emission index in kg/MWh is calculated as:

$$CO_2\ index = \frac{CO_2\ used}{Heating\ and\ cooling\ generated} \quad (4)$$

The total system cost is categorized into three primary components: investment cost, operational cost, and maintenance cost.

$$Total\ cost = Investment\ cost + operational\ cost \quad (5)$$

The operational cost encompasses the maintenance costs and energy costs needed for system operation, including heating from the district heating network and electricity purchased from the national electricity grid. Fig. 7 depicts the temporal fluctuations in heating and electricity prices in Uppsala, Sweden (2023). Fig. 7(a) illustrates the heating costs purchased from the district heating network. In Sweden, the cost structure of district heating generally comprises two elements: the energy price, which is billed per MWh of heat used, and a peak power cost for business customers, represented as a fixed annual fee determined by the maximum hourly heat demand, expressed in SEK/kW/year. This peak component highlights the importance of ensuring sufficient heating capacity during cold periods, which can significantly impact annual heating expenses. The maximum hourly demand determines the fixed peak power cost and functions similarly to a transmission or capacity reservation fee. This effective power charge substantially influences the annual district heating cost, as it dictates the extent of heating infrastructure capacity allocated for the building. Consequently, minimizing peak loads, particularly in winter, can result in significant long-term savings. According to Fig. 7(a), the monthly district heating price exhibits a distinct seasonal trend, peaking at approximately 674 SEK/MWh from December to March and declining to around 275 SEK/MWh during the summer months (May to August). The figure also indicates that the fixed peak power cost equals 950 SEK/kW/year.

Electricity costs in Sweden comprise several components (see Fig. 7 (b) and Fig. 7(c)): the spot market price, which fluctuates hourly, a fixed subscription fee charged monthly in SEK, a transmission fee based on grid access measured in SEK/kWh, and an effect-based fee calculated in SEK/kW/month, depending on the user's peak power demand. Fig. 7(b) illustrates that the monthly spot electricity price in 2023 exhibits a less distinct seasonal pattern, with peak average values recorded in February and December (approximately 3018 SEK/MWh) and reduced prices (ranging from 503 to 704 SEK/MWh) during the summer and early fall months. Fig. 7(c) provides a detailed analysis of the hourly variation in spot electricity prices, indicating substantial daily cost fluctuations. Prices tend to increase during peak hours in the morning (7–9 a.m.) and evening (5–8 p.m.), corresponding with increased demand in both commercial and residential sectors. The patterns highlight the significance of demand-side flexibility and intelligent scheduling, particularly in heat pump systems. Their operation can be strategically adjusted during low-price hours, thereby reducing electricity costs and maintaining thermal comfort.

A Net Present Value (NPV) analysis is conducted to evaluate the long-term financial viability of each system. NPV is a widely recognized economic measure employed to assess the cumulative value of a sequence of cash flows over time, incorporating the time value of money. This study employs the NPV method to analyze the cumulative cost differential between the proposed and alternative systems over a 20-year timeframe, assuming an interest rate of 10 %. This analysis helps determine the payback period, which is the year when accumulated savings exceed the initial investment. A positive NPV signifies that the system is financially advantageous throughout its lifecycle, whereas a negative NPV indicates a lack of economic viability based on the specified assumptions. When cumulative discounted savings turn positive, the year is designated as the payback period, serving as a valuable metric for investment recovery.

$$Net\ present\ value = \sum_{n=1}^{20} \frac{Product - (Operational)}{(1 + interest\ rate)^n} - Initial \quad (6)$$

A master flowchart is presented in Fig. 8 to provide readers with a comprehensive understanding of the current study. The roadmap-style flowchart outlines the sequential phases of the research, starting with

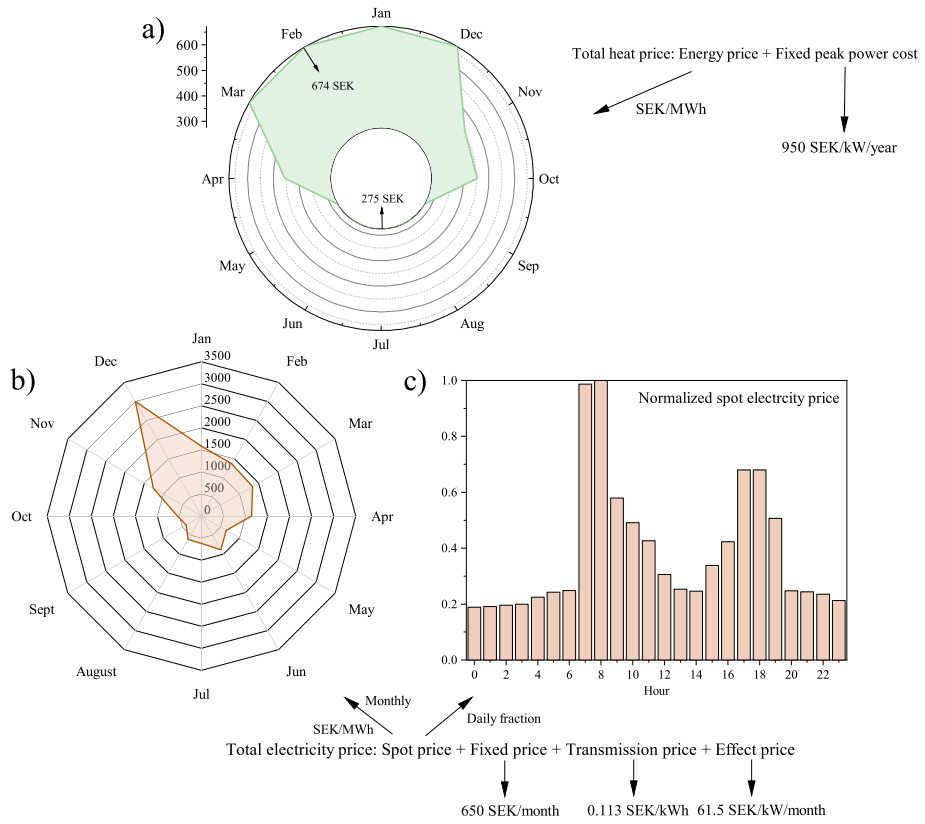

Fig. 7. a) averaged Monthly heating price (SEK/MWh), b) averaged monthly spot electricity price (SEK/MWh), and c) hourly spot electricity price fraction (normalized) [39,40].

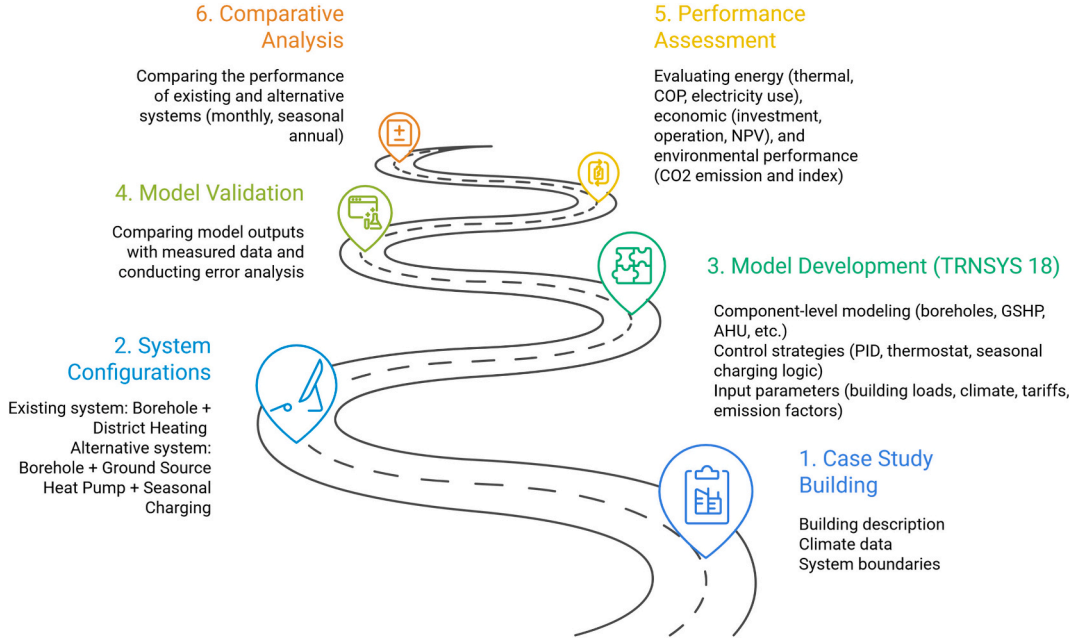

Fig. 8. Master flowchart illustrating the overall workflow of the study.

the characterization of the case study building (location, climate data, and system boundaries) and the specification of two alternative system configurations: the current borehole–district heating system and the proposed borehole–ground source heat pump system with seasonal charging. The workflow proceeds to model development in TRNSYS 18, where component-level dynamics, control techniques, and boundary conditions are defined. This is followed by model validation against measurement data from the building and borehole. The performance assessment thereafter assesses the systems from energy, economic, and environmental aspects, including thermal efficiency, coefficient of performance, investment and operational expenses, payback period, and CO_2 emissions. A comparative analysis combines the results to

emphasize trade-offs and long-term consequences.

3. Validation

A validation study is performed to confirm the accuracy and reliability of the simulation model created in TRNSYS, utilizing measurement data from the building management system (Tekla). The validation emphasizes two main elements: the building and the boreholes. Fig. 9 illustrates a heatmap depicting the daily relative error (%) between the building's simulated and measured thermal demands (heating + cooling). This figure presents a detailed overview of model accuracy across various months and days. The model demonstrates significant agreement, especially during the heating season when thermal demand is more stable and prevalent. Higher deviations are noted during the shoulder months (spring and autumn), likely due to unpredictable occupancy patterns or rapidly changing outdoor conditions. The distribution of relative errors remains within acceptable limits, indicating that the simulation accurately represents the building's dynamic thermal behavior.

Fig. 10 depicts the scatter plot comparing the daily simulated and measured heat extracted from or injected into the boreholes. The data points are tightly grouped around the reference line, signifying robust harmony between the model and real system performance. Two principal statistical indicators are computed: the root mean square error (RMSE) is roughly 132 kWh, and the coefficient of determination (R^2) is 0.985. These measures indicate that the simulation model strongly correlates with the measured data, capturing nearly all the variance in borehole performance. Furthermore, the average prediction error of 132 kWh/day is negligible, particularly in light of the substantial daily heating and cooling demands of commercial buildings, thereby reinforcing the model's trustworthiness.

4. Results and discussion

This section thoroughly analyzes and compares the performance of the existing borehole-district heating system with the proposed configuration that integrates a ground source heat pump. The analysis examines essential techno-economic and environmental indicators, including

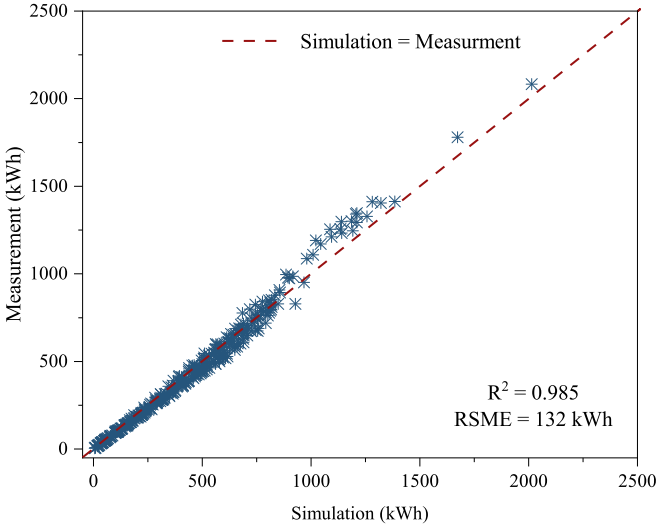

Fig. 10. The scatter plot simulation vs. measurement of daily heat extracted/injected from/into boreholes [41,42].

heating/cooling production, dependence on the district heating network, electricity use, coefficient of performance of the heat pump, heating costs, payback time, CO_2 emissions, and others.

4.1. Energy performance and system dynamics

To begin with, Fig. 11 and Fig. 12 comprehensively compare both systems' heating, cooling, and electricity flows through the Sankey diagram. It includes production, storage, usage, and buying among various components, as well as building and heating/electricity networks. According to Fig. 11, the district heating network primarily fulfills the heating demand in the existing system, supplying 721.5 MWh to radiators and 34.2 MWh to post-heating coils. Furthermore, 140 MWh of heat is withdrawn from the boreholes for preheating coils, thereby reducing dependence on the district heating network to a certain degree.

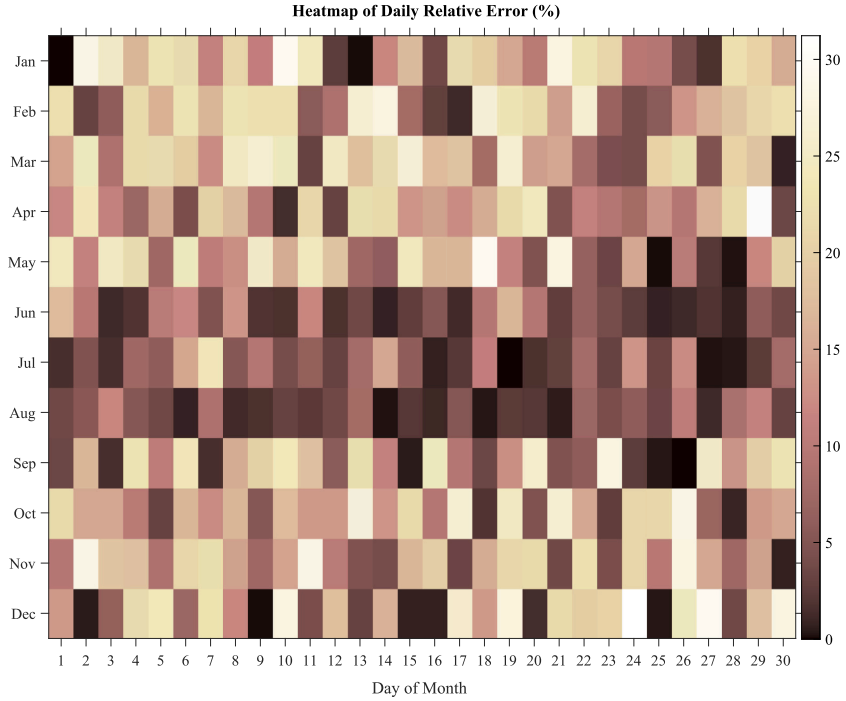

Fig. 9. The heatmap of daily relative error between the simulation and measurement of the building's thermal demand [41,42].

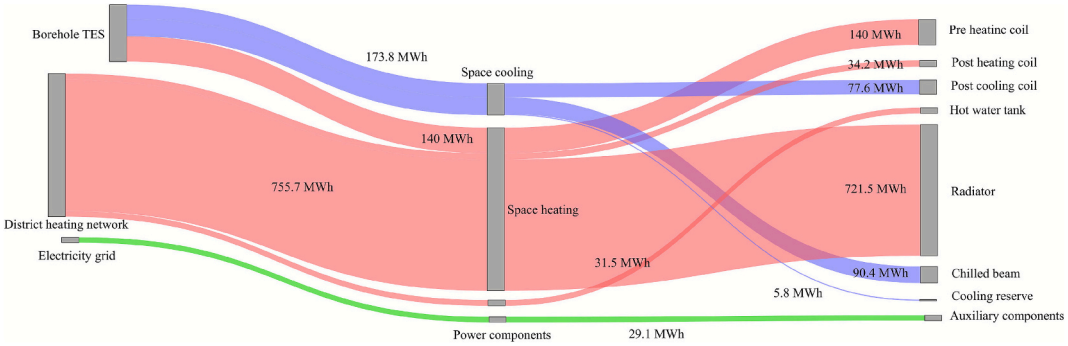

Fig. 11. The annual Sankey diagram of heating, cooling, and electricity flow in the existing system in Juvelen.

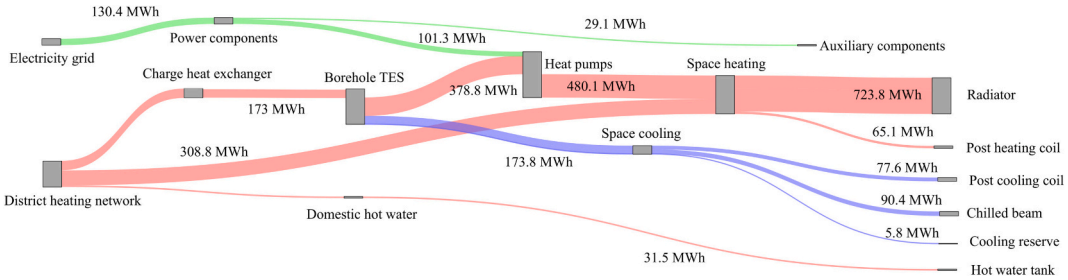

Fig. 12. The annual Sankey diagram of heating, cooling, and electricity flow in the alternative system based on the ground source heat pump supplemented by the DH.

Nonetheless, the absence of a heat pump means the DH network is the primary heating source. Cooling in both models is the same (see Fig. 11 and Fig. 12), with 90.4 MWh for chilled beams, 77.6 MWh for post-cooling coils, and 5.8 MWh allocated as a cooling reserve. In this system, electricity bought from the grid is only used to run auxiliary components like pumps and air handling units, totaling 29.1 MWh.

Compared to Fig. 11, Fig. 12 demonstrates that adding the heat pump markedly decreases dependence on the DH network for space heating, providing only 260.7 MWh to radiators (a substantial decrease from 721.5 MWh in the existing system) and 48.1 MWh to post-heating coils. The heat pump extracts 378.8 MWh of heat from the borehole thermal energy storage to supply radiators. However, this results in increased electricity purchased from the grid, requiring 101.3 MWh for the heat pump operation and an additional 29.1 MWh for other components. A closer look at the figure reveals that in September, 173.03 MWh of heat was supplied to the borehole from the district heating network to maintain thermal balance and ensure the long-term stability of ground temperature levels. The figures further show that the district heating network provides the entire domestic hot water demand of 31.5 MWh in both systems. According to the comparison of the borehole mechanisms in Fig. 11 and Fig. 12, the thermal balance in the boreholes in the alternative system is achieved. This improvement is due to the net heating removal/storage of boreholes approaching zero (33.8 MWh in the existing system vs. 32 MWh in the alternative system). The figure further illustrates that despite the rise in electricity usage, the heat pump enhances heat extraction efficiency from boreholes, thereby decreasing reliance on district heating and resulting in higher exploitation of green heating from the ground.

Fig. 13 compares the purchased heat to better understand both systems on the district heating network in different months. The monthly values indicate substantial decreases in DH demand because of the heat pump operation. In the existing system, district heating purchases remain consistently high throughout the heating season, reaching a peak of 127.4 MWh in February and 117.5 MWh in December and January.

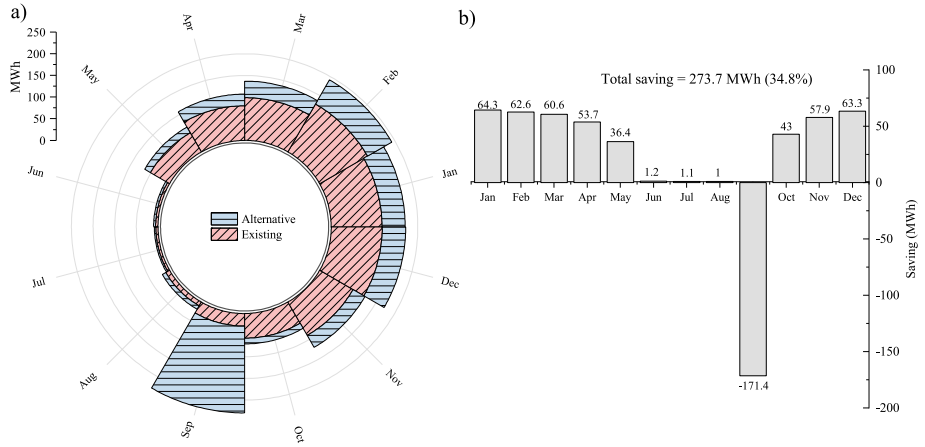

Fig. 13. a) The monthly comparison of the total heat bought from the district heating network in both models, and b) the monthly heat saved.

Heating demand decreases progressively during spring and summer, reaching its lowest levels in July (4.7 MWh) and June (5.5 MWh) to meet the domestic hot water need. In the heat pump integrated system, the total heat demand from district heating remains consistently lower during the heating season, with reductions varying from 30 % to 50 %, depending on the month. The most significant absolute savings are observed in January, February, and December, with heat savings exceeding 62–64 MWh per month.

According to Fig. 13(b), a distinct trend is observed in September, as the system with the heat pump exhibits a negative heat buy of −171.4 MWh, indicating that heat is being injected into the borehole thermal energy storage to maintain seasonal equilibrium. This strategy ensures adequate heat storage for future extraction, thanks to the increased operation of the heat pump, which extracts more heat from the ground compared to the existing system without a heat pump. This seasonal charging strategy is crucial for maintaining the effectiveness of boreholes throughout the year; however, it creates an additional peak in heat demand that adversely impacts the system's economics, primarily due to the district heating peak power cost, which is a fixed annual fee determined by the highest hourly demand. Consequently, the heightened peak in September may counterbalance some financial advantages despite the energy savings achieved. The charging process utilizes district heating rather than electricity. Consequently, no additional peak demand for electricity or time-of-use penalty is added. This finding highlights the importance of carefully planning seasonal charging events, particularly in systems where electric-based charging may be considered in the future. Aligning charging operations with off-peak electricity periods can enhance cost efficiency, particularly in markets characterized by dynamic electricity tariffs or demand charges. Finally, the figure shows that the total heating bought is saved more than 270 MWh (34.8 % relative reduction).

Fig. 14 illustrates the monthly changes in the share of each subsystem from the total heating purchased from the district heating network, providing a closer look at the operation of the existing system. In the winter months of January to March and November to December, radiator demand reaches its highest levels, surpassing 91 MWh in March and reaching up to 115 MWh in February. This trend is anticipated, as radiators are the primary source for sustaining indoor thermal comfort. During these months, the post-heating coils require additional heating to reach the air supply temperature that enters the building, achieving the desired values based on smart controls, albeit at a reduced scale (between 2.2 and 9.2 MWh) compared to radiators. The demand for domestic hot water exhibits relative constancy over the year, with minor fluctuations indicative of stable consumption patterns within the commercial buildings. The figure further shows that radiator heating demand decreases considerably in the warmer months of May through September, peaking in July (1.89 MWh), when little space heating is needed. Because no extra warming of supply air is required, post-heating coil use is totally eliminated from June to September. The demand for DHW, however, stays constant throughout, as anticipated.

Fig. 15 illustrates the monthly variation in heating purchased from the district heating network in the alternative system based on a ground source heat pump. The comparison of Fig. 14 and Fig. 15 depicts that the addition of a ground source heat pump within the system significantly decreases the district heating demand for radiator heating while increasing the need for post-heating coils. During the winter months, the demand for radiator DH in the GSHP system decreases by 60–80 % relative to the existing system, with January's demand falling from 107.7 MWh to 38 MWh and February's from 115.3 MWh to 48.8 MWh. This is rational because the heat pump extracts a greater amount of energy from the borehole thermal energy storage, thereby reducing dependence on district heating for space heating. However, because the boreholes no longer provide preheating coils, the post-heating coils require more heat from the network, increasing from 7.2 MWh to 12.5 MWh in January and from 9.2 MWh to 13.1 MWh in February. Domestic hot water demand is consistent across both systems, as it is not influenced by space heating and is mainly determined by user consumption.

In September, a significant spike in DH usage is observed. This phenomenon is attributable not to space heating demand but to a deliberate seasonal borehole charging operation. To maintain long-term thermal equilibrium, 173 MWh of heating is intentionally injected into the boreholes in September when district heating energy is less expensive and environmental conditions are optimal due to the increased heat extraction by heat pumps during winter. This singular injection, regulated by a PID controller, reinstates the average borehole temperature to its baseline and guarantees the thermal sustainability of the system throughout the heating and cooling seasons.

The monthly comparison of electricity bought from the grid to run each system is shown in Fig. 16. Implementing a ground-source heat pump significantly increases electricity usage, as the system requires power to operate the heat pumps for space heating purposes. In the existing system, electricity usage is consistently low throughout the year, primarily restricted to auxiliary components such as pumps and air handling units. The peak monthly electricity demand in the existing system occurs in February, reaching approximately 3.44 MWh. In contrast, during the summer months of June to August, demand decreases to below 1 MWh, indicating reduced electricity needs when heating is unnecessary.

On the other hand, the alternative system demonstrates a marked increase in power use, especially during winter when heat pumps

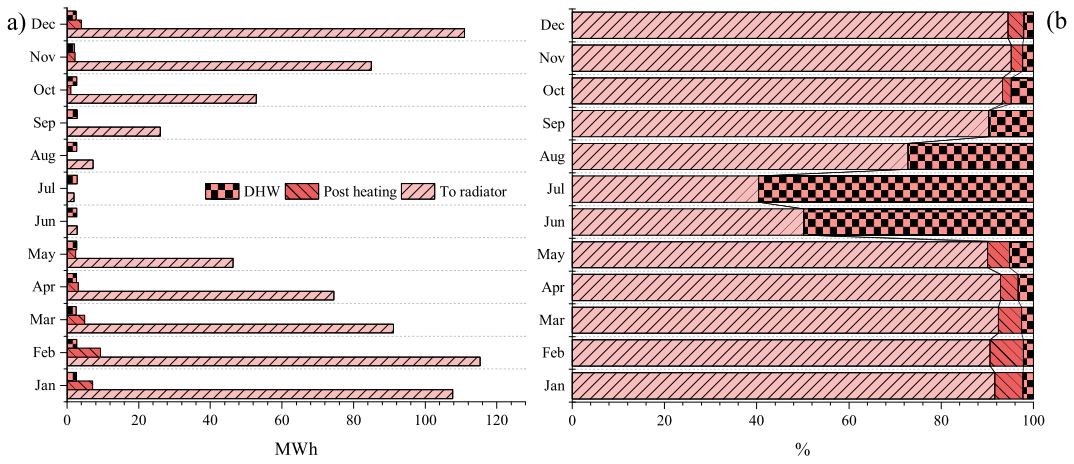

Fig. 14. Monthly contribution of each component to the heating demand supplied by the district heating network in the existing Juvelen system: (a) absolute values in MWh and (b) relative shares in percentage.

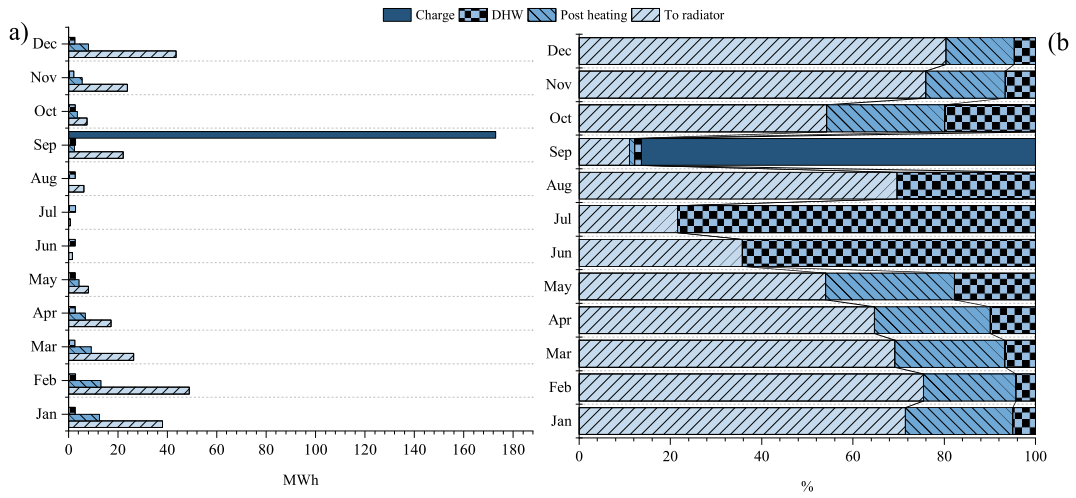

Fig. 15. Monthly contribution of each component to the heating demand supplied by the district heating network in the alternative system, which integrates ground source heat pumps: (a) absolute values in MWh and (b) relative shares in percentage.

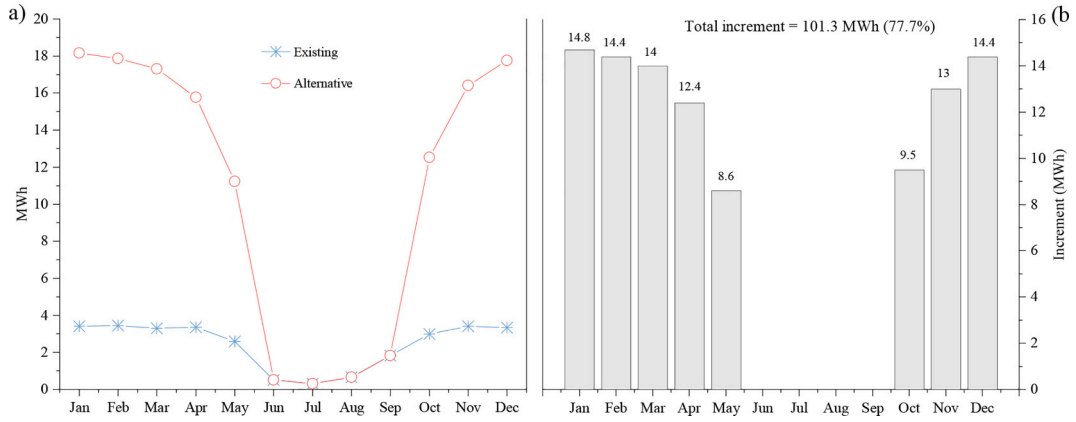

Fig. 16. Monthly comparison of total electricity purchased from the grid: (a) absolute electricity use in the existing and alternative models, and (b) relative increase in the alternative configuration.

operate more to extract heat from the borehole. The highest electricity demand is recorded in January (18.2 MWh), February (17.9 MWh), and December (17.8 MWh), with monthly electricity usage rising by 14–15 MWh relative to the existing system. In transitional months, such as October and April, the rise remains significant but less pronounced than during the peak winter months. The figure further shows that in the warmer months, both systems buy the same values of electricity from the grid due to the same cooling cycle operation.

In the proposed alternative system, the operation of the two 40 kW heat pumps is dynamically regulated according to the radiator heating demand to enhance energy efficiency and sustain indoor thermal comfort at 22 °C. To maximize system efficiency, the control strategy prioritizes the full-load operation of a single heat pump since heat pumps, like fans and pumps, typically achieve their highest coefficient of performance when operating close to their design point. During periods of moderate heating demand, one heat pump operates at full capacity while the second remains off to avoid inefficient part-load conditions. Both heat pumps are activated simultaneously during peak demand periods to meet the load. This approach ensures better alignment with the heat pumps' optimal efficiency range and reduces unnecessary electricity usage. Both heat pumps are turned off during periods of minimal heating demand, and the district heating network supplies the system exclusively. Fig. 17 illustrates the monthly variation in heat pump operation, detailing the number of hours each unit operates actively. This analysis examines seasonal variations in heating demand

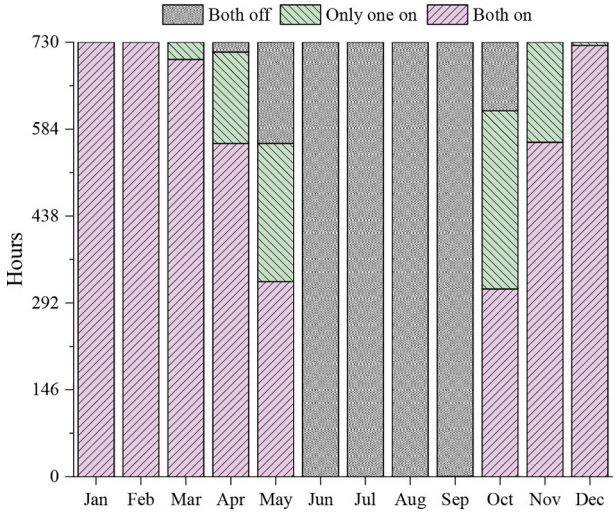

Fig. 17. The monthly changes in heat pump operation.

and evaluates its impact on the designed control strategy. According to the figure, both heat pumps operate at full capacity for 730 h a month (100 % uptime) during the peak heating months of January and

February, ensuring an adequate supply of heating to meet the building's demands. During transitional months like March, both heat pumps remain operational for most of the time, 701 h. The second heat pump, however, operates for only 29 h, reflecting brief intervals of reduced demand.

Furthermore, the figure shows that in the warmer months (June–August), both heat pumps are entirely inactive (730 h off every month) as space heating is not required, and the system depends solely on passive cooling via boreholes. The transition months (April, May, and October) exhibit a combination of operational modes characterized by an increase in partial load operation. For example, in May, a single heat pump operates for 232 h, whereas both heat pumps function for 328 h, indicating reduced heating demand. In October, the heat pumps function more balanced, with 315.5 h of full load and 299.5 h of single-unit operation, as temperatures begin to decline. This pattern highlights the effectiveness of the control strategy in modulating heat pump operation according to seasonal demand, thereby optimizing efficiency and minimizing unnecessary electricity usage.

Fig. 18 presents the monthly performance metrics of the GSHP system, including the heat extracted from the borehole (source heat), electricity used by the compressor, heat delivered to the radiators (load), the COP, average outdoor air temperature, and average radiator supply temperature. Due to low outdoor temperatures, the heating load peaks in the coldest months, January, February, and December. In this period, the COP exhibits stability, averaging approximately 4.5 to 4.7. Although the heat demand is relatively high and stable during these months, continued heat extraction causes the ground loop temperature to gradually decrease, thereby reducing the temperature difference between the condenser and the evaporator. This leads to increased compressor work and decreased heat pump efficiency.

Conversely, the COP exhibits improvement during the transitional months of April, May, and particularly October. As heating demand diminishes and radiator supply temperatures are adjusted, the temperature differential between the condenser and evaporator decreases, thereby reducing the work required by the compressor. October demonstrates the highest COP (5), directly linked to the borehole charging that occurred in September. The seasonal heat injection raises ground temperature, improving evaporator inlet conditions before the heating season begins. Despite a decline in COP in November due to increased heating and cooling boreholes, the system exhibits relatively high performance year-round. The observations indicate that the smart integration strategy, which includes seasonal borehole balancing, markedly improves the energy efficiency and operational stability of the GSHP system.

4.2. Economic feasibility and lifecycle costing

Fig. 19 illustrates the investment costs by presenting and comparing the initial costs of each subsystem for both models. The investment costs associated with boreholes, chilled beams, and energy wheels are the same across both existing and alternative systems, as these components operate similarly in each configuration. As depicted, the borehole system, representing the largest investment, is valued at 2,238,853 SEK. Furthermore, energy wheels employed for heat recovery are 514,912 SEK across both models. The alternative system needs further investment in particular components, resulting in an overall increase of 11.1 % in total investment costs. The primary addition is the heat pump, which costs 347,875 SEK and is not in the existing system. This constitutes the fundamental aspect of the new system's heating strategy, facilitating a decrease in district heating usage over time, as well as the increased deployment of boreholes, which have such high initial costs.

The figure further illustrates that the additional cost variations arise from the modifications necessary to integrate the heat pump. The cost of the hydronic system, including valves, fans, pumps, controllers, and other components, increases from 67,402 SEK to 171,271 SEK. This increase is attributed to the need for additional piping, circulation pumps, and system controllers to enhance the heat pump's functionality. Furthermore, the costs associated with heat exchangers increased by 9.9 %, rising from 49,287 SEK to 54,173 SEK, due to the addition of a heat

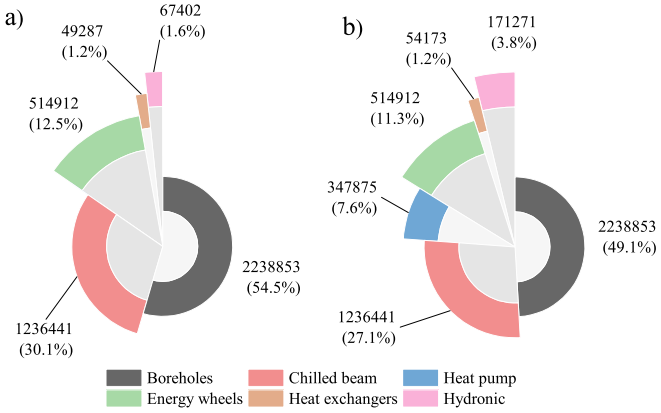

Fig. 19. Comparison of the investment cost distribution across subsystems: (a) the existing system in Juvelen and (b) the alternative configuration with ground source heat pump integration.

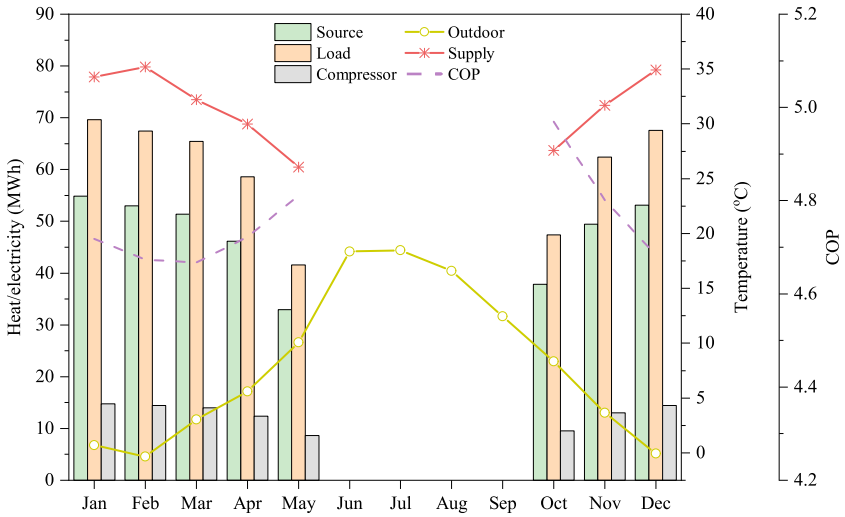

Fig. 18. The monthly changes in key heat pump's indicators and the outdoor and radiator supply temperatures.

exchanger to charge the boreholes from DH in September. Long-term operational savings resulting from decreased heating costs and enhanced efficiency justify the enhanced initial investment. Despite the initial financial increase, the alternative system offers a more sustainable and cost-effective solution, with reduced operational costs and a shorter payback time.

Table 3 compares the key metrics, including investment cost, cost of purchased heat, cost of purchased electricity, maintenance and operational costs, LCOE, CO_2 used and index, and Payback time. The economic analysis indicates that the alternative system requires a greater initial investment (4,563,518 SEK compared to 4,106,894 SEK, an increase of 11.1 %), yet it provides significant savings in operational costs, especially regarding district heating costs. According to the table, the total cost of purchased heat (energy+power) declined by 29 %, from 740,224 SEK to 524,156 SEK. This reduction is primarily attributed to a 49 % decrease in energy-related heat costs, demonstrating the heat pump's capacity to extract heat from borehole thermal energy storage. Despite the decrease, the power-related DH cost rose by 9 %, increasing from 187,896 SEK to 204,057 SEK. The increase is attributed to a new peak in heating demand in September, when heat is purchased from the district heating network to recharge the boreholes and maintain their thermal balance. It demonstrates that this approach enhances system sustainability but has an adverse impact on peak-based pricing.

Simultaneously, costs associated with electricity increase markedly as a result of heat pump operation. The total electricity costs have risen 4.3 times, from 31,425 SEK to 135,816 SEK. This increase includes a 4.5-fold rise in spot market costs and a 9.8-fold increase in effect-based electricity fees, indicative of increased peak electrical loads. Maintenance costs rise by 11.1 %; however, the total operational cost declines by 9 %, suggesting enhanced cost-effectiveness in long-term operations. The total annual cost, including investment and operation, rises by 7.2 % (from 5,083,888 SEK to 5,451,661 SEK). The payback period decreases marginally from 10.9 to 10.5 years due to recurring savings in heat energy costs.

The table further shows that the alternative system demonstrates superior environmental performance compared to existing systems by markedly decreasing CO_2 emissions. The annual total CO_2 used decreased from 38.3 to 26.9 t, representing a 29.8 % reduction. The CO_2 index per heating/cooling unit was also enhanced by 35.1 %, changing from 34.8 to 22.6 kg/MWh. This illustrates the heat pump's capacity to deliver cleaner energy by reducing dependence on the electricity grid, which is greener than the district heating network in Sweden. In essence, despite the alternative system's increased initial and electricity costs, its reduced heating expenses, environmental advantages, and enhanced payback period make it a more economically viable and sustainable option over time. However, it may increase exergy losses relative to the original configuration. This arises from the compression process of the heat pump and the additional heat exchanger for borehole recharging from district heating in September. The objective of this study is not to minimize exergy loss, but rather to achieve practical, clever integration and smart seasonal energy management for further cost reduction and environmental benefits. The electricity powering the heat pump in Sweden is predominantly derived from fossil-free sources, and the enhanced ground heat extraction leads to a 76 % increase in the utilization of renewable energy. Consequently, despite the exergy penalty, the alternative system presents a feasible and climate-aligned enhancement compared to the existing configuration.

Table 3
The comparison of the main economic and environmental metrics of the existing system against the alternative system based on the ground source heat pump.

Indicator	Unit	Existing	Alternative	Relative increase/ decrease (%)
Investment cost	[SEK]	4,106,894	4,563,518	11.1
Cost of purchased heat (energy)	[SEK]	471,381	239,156	−49
Cost of purchased heat (power)	[SEK]	268,843	285,000	6
Total cost of purchased heat	[SEK]	740,224	524,156	−29
Cost of purchased electricity (spot)	[SEK]	16,337	73,921	+4.5 times
Cost of purchased electricity (fixed)	[SEK]	7800	7800	0
Cost of purchased electricity (transmission)	[SEK]	3288	14,735	+4.4 times
Cost of purchased electricity (effect)	[SEK]	4000	39,360	+9.8 times
Total cost of purchased electricity	[SEK]	31,425	135,816	+4.3 times
Maintenance cost	[SEK]	205,345	228,171	11.1
Operational cost	[SEK]	976,994	888,143	−9
Total cost	[SEK]	5,083,888	5,451,661	7.2
LCOE	[SEK. MWh^{-1}]	4527	4804	6
CO_2 used	[Tonne]	38.3	26.9	−29.8
CO_2 index	[kg. MWh^{-1}]	34.8	22.6	−35.1
Payback time	Year]	10.9	10.5	−4

Fig. 20 illustrates the long-term financial comparison of both systems to see how they perform over 20 years after installation. The net present value analysis over two decades underscores the long-term financial benefits of the alternative system, albeit with its increased initial cost. At time zero, the existing system meets with an investment of 4,106,894 SEK, whereas the alternative system costs 4,563,518 SEK, indicating 11.1 % greater initial costs. As operational savings grow, the budgetary gap between the two models diminishes considerably over time. By year 10.5, the alternative system achieves break-even, attaining a positive NPV, whereas the existing system requires 10.9 years to reach the same threshold. The reduced payback period for the alternative system underscores its cost-effectiveness, demonstrating that diminished operational costs result in swifter returns despite the elevated initial expenses.

After the payback period, the alternative system exhibits enhanced long-term financial sustainability. By year 20, the system achieves a net present value of 1,586,230 SEK, compared to 1,321,804 SEK for the existing system, indicating an almost 20 % difference in long-term profitability compared to the existing system. This signifies that the alternative system not only recoups its investment more rapidly but also consistently yields enhanced financial advantages over time.

Fig. 21 compares the payback time and profit variation after 20 years for both systems, varying the interest rate. With the rise in interest rates from 6 % to 12 %, both systems encounter prolonged payback periods and diminished profitability. The alternative system consistently performs better than the existing configuration across all interest rates. The alternative system, at a discount rate of 6 %, results in a payback period of 8.18 years and a profit of approximately 3,720,000 SEK, whereas the existing system yields a payback period of 8.41 years and a profit of 3,190,000 SEK. Under a 12 % interest rate, the alternative model demonstrates financial viability, exhibiting a payback period of 12.54 years and a profit of 830,000 SEK, surpassing the existing system's payback period of 13.15 years and profit of 650,000 SEK. The robustness of the alternative system underscores its superior long-term economic performance and enhanced resilience to financial uncertainty, thereby confirming its suitability for smart, low-carbon HVAC retrofits. Future research could extend this analysis by incorporating uncertainties related to energy prices, building load variations, and ground temperature fluctuations, thereby facilitating a more probabilistic assessment of system performance.

4.3. Carbon footprints

In order to compare both systems' environmental facets, Fig. 22 comprehensively investigates the monthly changes in CO_2 used and the

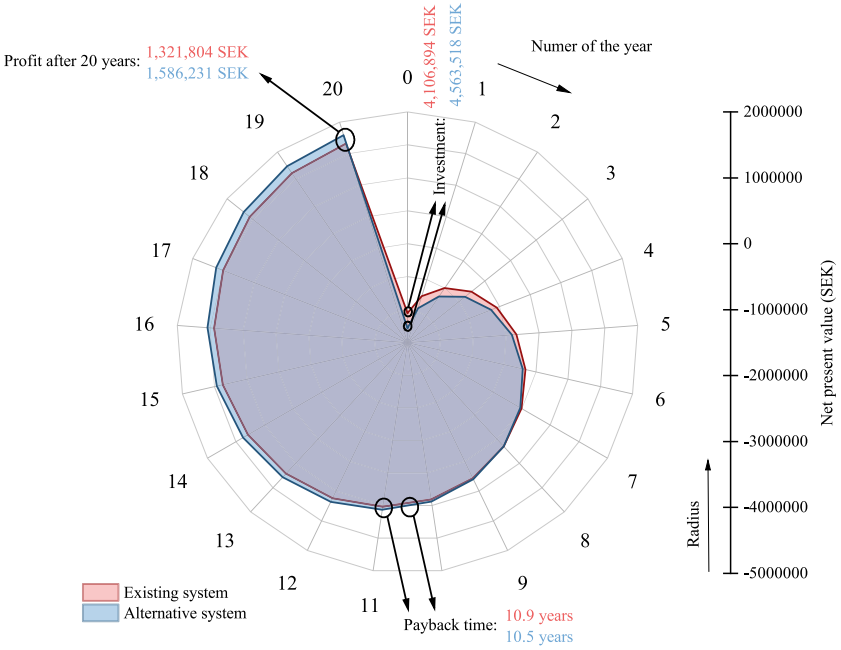

Fig. 20. The comparison of the net present value and payback period of the existing system and the alternative system based on the ground source heat pump.

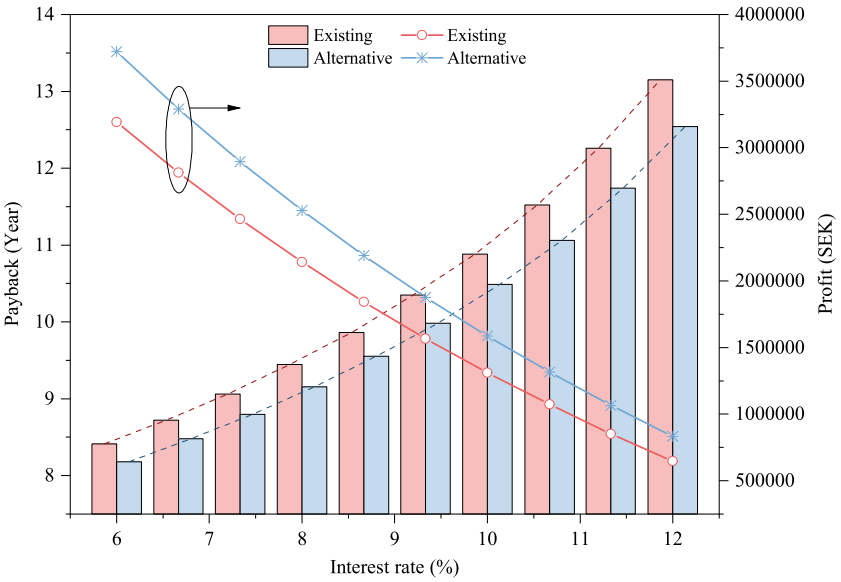

Fig. 21. The sensitivity analysis: variation of payback time and profit over the investment horizon with the interest rate for both systems.

usage differences. According to the figure, the trends in CO_2 emissions for both configurations underscore the substantial environmental advantages of incorporating borehole thermal energy storage as a deep green heating and cooling resource. In the existing system (Fig. 22(a)), CO_2 emissions reach their maximum during the winter months, peaking at 5.9 t in February and 5.6 t in January and December, primarily due to a significant dependence on district heating for space heating. Emissions progressively decrease in spring and summer, reaching their lowest point in June (0.4 t) and July (0.3 t), when heating demand is minimal.

Conversely, the alternative system (Fig. 22(b)) exhibits markedly reduced CO_2 emissions year-round, particularly during winter. Emissions peak in February (3.4 t), January (2.9 t), and December (3.0 t), representing nearly a 50 % reduction compared to the existing system. The system's increased dependence on electricity rather than district heating leads to reduced carbon intensity, while the heat pump's superior efficiency reduces CO_2 emissions per unit of heat generated. The most notable distinction occurs in September, when the alternative system demonstrates a negative CO_2 impact of −6.57 t (Fig. 22(c)), due to heat being transferred into the borehole TES, which efficiently stores low-carbon and cheaper heat for further utilization. The yearly decrease in CO_2 emissions, from 38.3 to 26.9 tons (approximately 30 % lower), demonstrates the ongoing environmental benefits of the alternative system, making it a more sustainable option for heating and cooling while advancing climate objectives.

Fig. 23 presents a detailed comparison of CO_2 emissions between the existing system and the alternative system, including the annual carbon dioxide savings resulting from renewable utilization and the annual usage associated with purchasing electricity/heating from the grid. The existing system utilizes 313.8 MWh of renewable energy yet generates 38.3 t of CO_2 per year, resulting in a net CO_2 effect of 23.9 tons after

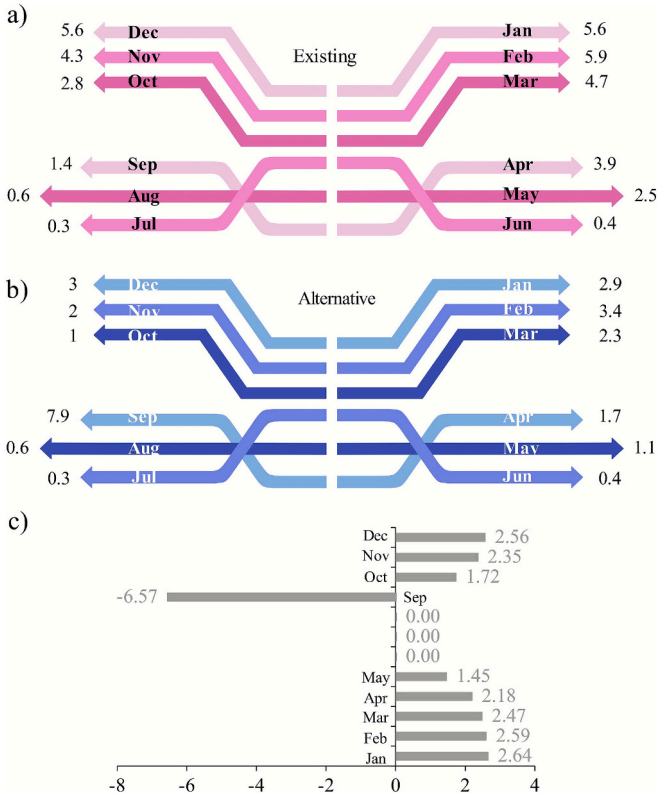

Fig. 22. Monthly CO_2 emissions of (a) the existing system, (b) the alternative system with ground source heat pump integration, and (c) the monthly differences in CO_2 emissions between the two configurations (in tonnes).

considering savings.

On the other hand, the alternative system exhibits markedly enhanced carbon efficiency, utilizing 552.6 MWh of renewable energy through borehole TES and reducing annual CO_2 emissions to 26.9 t, resulting in a net CO_2 effect of only 1.6 t. This is primarily due to the superior energy efficiency of the heat pump, which recovers more heat from renewable borehole thermal energy storage and reduces dependence on district heating. This system reduces CO_2 emissions by 25.3 t annually, approximately twice the reduction achieved by the existing system (14.4 t per year). The figure suggests that the alternative system aligns more closely with zero-emission objectives, interpreting it as a more sustainable and environmentally friendly option for heating and cooling applications.

5. Conclusions

This article introduces a cutting-edge smart heating and cooling solution designed to further reduce operational costs and CO2 emissions while enhancing energy conversion in commercial buildings, including offices and a restaurant in Uppsala, Sweden. The concept's heart is an innovative yet smart strategy of integrating a heat pump into borehole thermal energy storage to further harness the ground's natural heat potential. After performing a techno-environmental and economic assessment, a comprehensive comparison of the proposed solution is conducted against the existing system, which primarily relies on the district heating network and natural ground heating and cooling. The key outcomes could be outlined as follows:

- The alternative system substantially reduces reliance on district heating by shifting heating demand to borehole thermal energy storage through the integration of heat pumps. Although electricity use increases and leads to a modest 6 % rise in the cost of purchased heat (power), the high efficiency of the GSHP offsets these expenses. Overall, total operational costs are reduced by approximately 9 %, and the net present value improves by around 20 % over a 20-year period.
- A second key difference is in borehole performance. By applying a seasonal charging strategy in September, the system offsets the additional extraction from the ground source heat pump, prevents long-term ground temperature depletion, and achieves a more balanced thermal profile compared to the existing system.
- From an environmental perspective, the benefits are even more striking. The heat pump integration enhances borehole utilization, increases renewable energy contribution, and cuts net CO_2 emissions by about 93 % compared to the existing system, fully supporting Sweden's net-zero targets.

While the findings confirm the potential of GSHP–BTES integration, several limitations should be acknowledged.

- The operational cost savings are highly sensitive to peak heat (power) tariffs. Policymakers have designed this factor, which is expected to rise. Therefore, the long-term viability of heat pump integration depends not only on technical performance and CO_2 reductions, but also on the development of local energy price structures.
- The results are context-specific, as they rely on Sweden's green electricity mix and unique tariff structure; therefore, the outcomes cannot be directly generalized to other countries with different grid carbon intensities or pricing structures.
- The modeling framework captures system dynamics with validated TRNSYS components. However, real-world operational uncertainties, such as occupant behavior, extreme weather events, and equipment degradation, remain beyond the present scope.

Building on these findings, future research could include the assessment of different building typologies and climatic contexts to test the broader applicability of the results. It could also analyze the uncertainty and sensitivity testing on tariffs, policy shifts, and climate variability to assess the robustness of techno-economic results. The deployment of advanced predictive controllers, such as forecast-driven

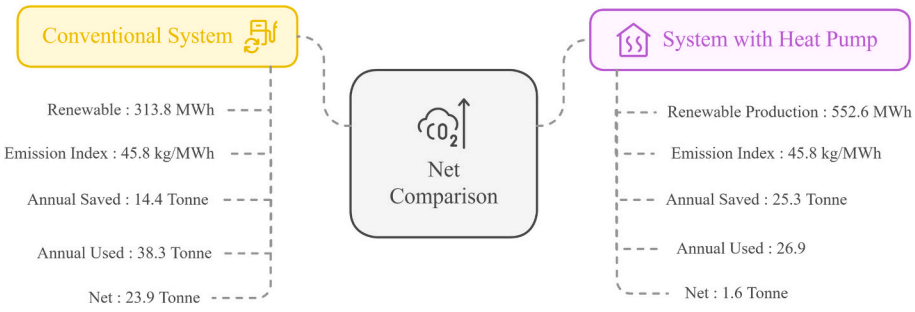

Fig. 23. The detailed CO_2 emission comparison of the existing system against the alternative system based on the ground source heat pump.

control, could be another suggestion to optimize system operation by using hourly electricity price variability and managing seasonal thermal balance more intelligently.

CRediT authorship contribution statement

Amirmohammad Behzadi: Writing – original draft, Visualization, Validation, Software, Methodology, Investigation, Formal analysis, Conceptualization. **Taha Arghand:** Writing – review & editing, Validation, Supervision, Methodology, Data curation. **Christophe Duwig:** Writing – review & editing, Supervision, Funding acquisition, Data curation, Conceptualization. **Hailong Li:** Writing – review & editing, Validation, Supervision, Data curation, Conceptualization. **Sasan Sadrizadeh:** Writing – review & editing, Supervision, Resources, Project administration, Funding acquisition, Formal analysis.

Declaration of competing interest

The authors declare that they have no known competing financial interests or personal relationships that could have appeared to influence the work reported in this paper.

Acknowledgments

The authors are grateful to the Swedish Energy Agency (Energimyndigheten) for funding this research study within the Termo research program. This article is drafted in line with Annex 37: Smart Design and Control of Energy Storage Systems, which is under the umbrella of the International Energy Agency's Energy in Buildings and Communities Programme (IEA EBC). We also extend our sincere gratitude to Vasakronan Real Estate Company for their kind contribution to building data, which was essential to the success of the simulation. We acknowledge Vattenfall AB for its insights and background information regarding the district heating network and its integration with building systems. This article benefited from language refinement and editorial assistance using ChatGPT-5, an AI-powered language model developed by OpenAI. The tool was employed to improve clarity, coherence, and grammar throughout the text. The authors assume full responsibility for the content and accuracy of the text and data.

Appendix A. Appendix

To improve the reproducibility of the study, comprehensive input data and schedules implemented in TRNSYS simulations are presented in Tables A1–A4. The parameters include building envelope specifications, borehole and system details, occupancy and airflow schedules, and the technical aspects of the ground-source heat pump. Table A1 outlines the essential input parameters necessary for simulating the thermal dynamics of the building and the functioning of the HVAC system. The inputs are categorized into thermodynamic, heat transfer, thermo-physical, and occupancy-related parameters. According to the figure, the heat transfer fluid entering the borehole system is a 30/70 Ethylene Glycol/Water mixture, characterized by a density of 1048 kg/m^3 and a specific heat capacity of 3.6 kJ/(kg·K). Collectively, these variables establish the basis for thermal and energy modeling, guaranteeing a precise depiction of building performance in existing and alternative systems.

Table A1
The main input parameters to model the building and HVAC systems.

Parameter	Value	Parameter	Value
Room temperature (heating), °C	22	Air change (offices), 1/h	2
Room temperature (cooling), °C	24	Window ratio of north façade (%)	30
Window's heat lost coefficient, W/(m^2.K)	1	Concrete ratio of north façade (%)	70
Roof/floor's heat lost coefficient, W/(m^2.K)	0.65	Window ratio of east façade (%)	26
Wall's heat lost coefficient, W/(m^2.K)	0.6	Concrete ratio of east façade (%)	74
Total boreholes	25	Window ratio of southwest façade (%)	28
Occupant density (restaurant), m^2/person	6	Concrete ratio of southwest façade (%)	72
Occupant density (offices), m^2/person	17	The total depth of each borehole, m	250
Occupants' heat gain (restaurant), W/m^2	19.7	Space between each borehole, m	6
Occupants' heat gain (offices), W/m^2	7	The radius of each borehole, mm	70
Equipment's heat gain (restaurant), W/m^2	4	The outer/inner radius of the pipe, mm	16/14
Equipment's heat gain (offices), W/m^2	12	Fill thermal conductivity, W/(m.K)	0.8
Lightning's heat gain (restaurant), W/m^2	20	Fluid heat transfer coefficient kJ/(kg.K)	3.6
Lightning's heat gain (offices), W/m^2	12	The density of the fluid, kg/m^3	1048
Air change (restaurant), 1/h	6	The thermal conductivity of the pipe, W/(m.K)	0.38

Table A2 presents the hourly airflow schedule for the three air-handling unit lines in the proposed smart HVAC system, categorized by day type and zone. The system comprises Line 1 and Line 2, which serve office areas, and Line 3, which supplies the restaurant zone. The table presents detailed patterns for weekdays and weekends, indicating that Line 1 sustains a baseline night airflow of 5 m^3/s, which rises to 7.5 m^3/s during occupied daytime hours. Line 2 is inactive on weekends and increases from 0 to 7.5 m^3/s during weekdays, indicating occupancy-driven control. Line 3 exhibits significant variability, categorized by day type, with distinct patterns observed on Mondays and Tuesdays, Wednesdays and Thursdays, Fridays, Saturdays, and Sundays. Airflow reaches a maximum of 4.2 m^3/s during peak meal service hours. The schedules function as essential boundary conditions in the simulation model, determining thermal load distributions and ventilation energy needs across zones and time, thus affecting heating, cooling, and control logic in HVAC systems.

Table A2
The schedule detailing the air flowrate in m^3 per second entering air handling units.

Hour	Line 1		Line 2		Line 3				
	Week	Weekend	Week	Weekend	Monday&Tuesday	Wednesday&Thursday	Friday	Saturday	Sunday
0	5	5	0	0	0	0	0	0	0
1	5	5	0	0	0	0	0	0	0
2	5	5	0	0	0	0	0	0	0
3	5	5	0	0	0	0	0	0	0
4	5	5	0	0	0	0	0	0	0
5	5	5	0	0	0	0	0	0	0
6	7.5	5	7.5	0	0	0	0	0	0
7	7.5	5	7.5	0	0	0	0	0	0
8	7.5	5	7.5	0	0	0	0	0	0
9	7.5	5	7.5	0	4.2	4.2	4.2	0	0
10	7.5	5	7.5	0	4.2	4.2	4.2	0	0
11	7.5	5	7.5	0	4.2	4.2	4.2	0	0
12	7.5	5	7.5	0	4.2	4.2	4.2	4.2	4.2
13	7.5	5	7.5	0	4.2	4.2	4.2	4.2	4.2
14	7.5	5	7.5	0	4.2	4.2	4.2	4.2	4.2
15	7.5	5	7.5	0	4.2	4.2	4.2	4.2	4.2
16	7.5	5	7.5	0	4.2	4.2	4.2	4.2	4.2
17	7.5	5	7.5	0	2	4.2	2	4.2	4.2
18	7.5	5	7.5	0	2	4.2	2	2	2
19	7.5	5	7.5	0	0	4.2	2	2	2
20	7.5	5	7.5	0	0	4.2	4.2	4.2	0
21	5	5	0	0	0	4.2	4.2	4.2	0
22	5	5	0	0	0	4.2	4.2	4.2	0
23	5	5	0	0	0	2	2	2	0
24	5	5	0	0	0	2	2	2	0

Table A3 presents the technical specifications of the proposed ground source heat pump in the enhanced system configuration. The NIBE F1345 model is a water-to-water heat pump tailored for larger commercial applications and utilizes refrigerant R407C. The heat pump's performance is evaluated under various inlet brine and outlet heating temperature conditions. According to the table, under standard test conditions of 0/35 °C, the unit provides a heating capacity of 39.94 kW with a power input of 8.9 kW, resulting in a coefficient of performance (COP) of 4.49.

Table A3
The technical specifications of the proposed heat pump system [43].

Parameter	Value
Heating capacity (0/35), kW	39.94
Supplied power (0/35), kW	8.9
COP (0/35), –	4.49
Heating capacity (0/45), kW	38.9
Supplied power (0/45), kW	10.61
COP (0/45), –	3.67
Heating capacity (10/35), kW	51.71
Supplied power (10/35), kW	9.81
COP (10/35), –	5.27
Heating capacity (10/45), kW	50.79
Supplied power (10/45), kW	11.82
COP (10/45), –	4.3
Type of refrigerant	R407C
Max system pressure brine, MPa	0.6
Brine min flow, l/s	1.59
Brine nominal flow, l/s	2.09
Heating medium min flow, l/s	0.64
Heating medium nominal flow, l/s	0.93

Table A4 presents the working hour schedule for the office and restaurant zones, which is critical for precisely modeling internal heat gains, ventilation needs, and control logic across daily and weekly periods. The offices exhibit a weekday occupancy pattern, operating from 07:00 to 18:00 on weekdays and remaining closed on weekends, consistent with standard business practices. The restaurant's schedule exhibits greater variability, featuring extended weekday operating hours. Occupancy schedules have a significant impact on airflow setpoints, internal load profiles, and HVAC system operations, enabling a dynamic response to actual usage patterns across various building zones.

Table A4
The working hour schedule of the offices and the restaurant.

Hour	Offices		Restaurant			
	Week	Weekend	Monday&Tuesday	Wednesday - Friday	Saturday	Sunday
0	Closed	Closed	Closed	Closed	Closed	Closed
1	Closed	Closed	Closed	Closed	Closed	Closed
2	Closed	Closed	Closed	Closed	Closed	Closed
3	Closed	Closed	Closed	Closed	Closed	Closed
4	Closed	Closed	Closed	Closed	Closed	Closed
5	Closed	Closed	Closed	Closed	Closed	Closed
6	Closed	Closed	Closed	Closed	Closed	Closed
7	Open	Closed	Closed	Closed	Closed	Closed
8	Open	Closed	Open	Open	Closed	Closed
9	Open	Closed	Open	Open	Closed	Closed
10	Open	Closed	Open	Open	Closed	Closed
11	Open	Closed	Open	Open	Closed	Closed
12	Open	Closed	Open	Open	Closed	Closed
13	Open	Closed	Open	Open	Closed	Closed
14	Open	Closed	Open	Open	Closed	Closed
15	Open	Closed	Open	Open	Closed	Closed
16	Open	Closed	Open	Open	Closed	Closed
17	Open	Closed	Closed	Open	Closed	Closed
18	Open	Closed	Closed	Open	Open	Closed
19	Closed	Closed	Closed	Open	Open	Closed
20	Closed	Closed	Closed	Open	Open	Closed
21	Closed	Closed	Closed	Open	Open	Closed
22	Closed	Closed	Closed	Open	Open	Closed
23	Closed	Closed	Closed	Closed	Open	Closed
24	Closed	Closed	Closed	Closed	Closed	Closed

Fig. A1 illustrates the TRNSYS Studio schematics of the modeled system configurations. It includes the complete building energy system, including air handling units, zones, chilled beams, district heating exchangers, and borehole integration. Fig. A1(b) presents the existing borehole–district heating configuration. In this figure, boreholes are used in a direct free-heating/free-cooling mode without active seasonal management. Fig. A1(c) illustrates the proposed alternative configuration, featuring ground source heat pumps and a September charging strategy, which enables improved borehole utilization, higher efficiency, and long-term thermal balance.

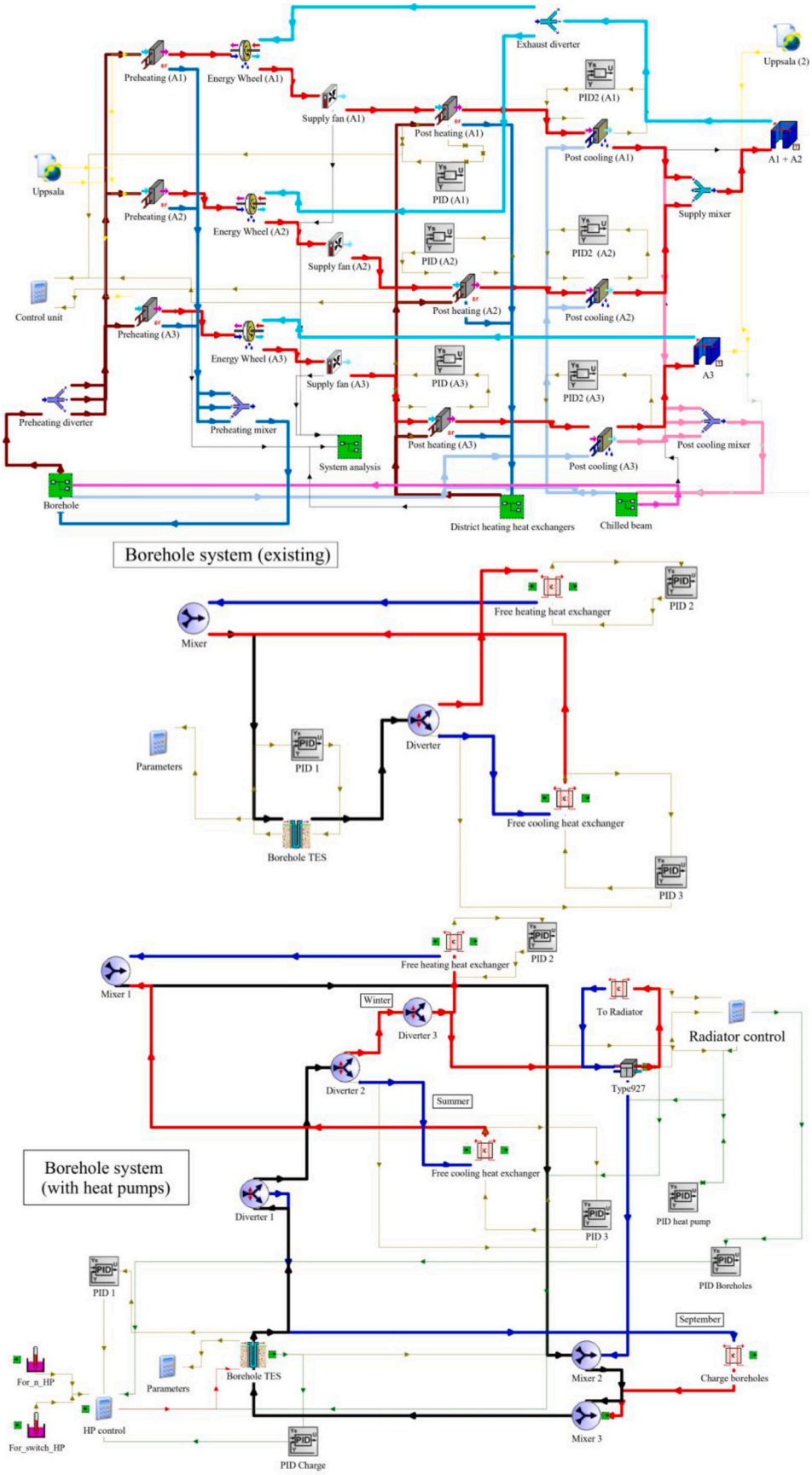

Fig. A1. TRNSYS Studio representation of the studied configurations: (a) overall building energy system, (b) existing system, and (c) alternative system with integrated heat pumps and seasonal charging strategy.

Data availability

Data will be made available on request.

References

[1] Sandvall A, Karlsson KB. Energy system and cost impacts of heat supply to low-energy buildings in Sweden. Energy 2023;268:126743. https://doi.org/10.1016/j.energy.2023.126743.

[2] Ekmekci E, Aydin M, Ozturk ZF, Sisman A. Very high temperature BTES: a potential for operationally cost-free and emission-free heating. Appl Energy 2024;360:122859. https://doi.org/10.1016/j.apenergy.2024.122859.

[3] Wang J, Wang Y, Qiu D, Su H, Strbac G, Gao Z. Resilient energy management of a multi-energy building under low-temperature district heating: a deep reinforcement learning approach. Appl Energy 2025;378:124780. https://doi.org/10.1016/j.apenergy.2024.124780.

[4] El Shamy AR, Al-Sumaiti AS. Optimal cost predictive BMS considering greywater recycling, responsive HVAC, and energy storage. Appl Energy 2025;377:124589. https://doi.org/10.1016/j.apenergy.2024.124589.

[5] Spitler D, Gehlin S. Commercial-Building Ground Source Heat Pump Energies 2020;12:34.

[6] Guo F, Zhu X, Zhang J, Yang X. Large-scale living laboratory of seasonal borehole thermal energy storage system for urban district heating. Appl Energy 2020;264:114763. https://doi.org/10.1016/j.apenergy.2020.114763.

[7] Shah SK, Aye L, Rismanchi B. Simulated performance of a borehole-coupled heat pump seasonal solar thermal storage system for space heating in cold climate. Sol Energy 2020;202:365–85. https://doi.org/10.1016/j.solener.2020.03.111.

[8] Giordano N, Raymond J. Alternative and sustainable heat production for drinking water needs in a subarctic climate (Nunavik, Canada): borehole thermal energy storage to reduce fossil fuel dependency in off-grid communities. Appl Energy 2019;252:113463. https://doi.org/10.1016/j.apenergy.2019.113463.

[9] Fiorentini M, Heer P, Baldini L. Design optimization of a district heating and cooling system with a borehole seasonal thermal energy storage. Energy 2023;262:125464. https://doi.org/10.1016/j.energy.2022.125464.

[10] Saitoh TS, Yamaguchi A. Efficient borehole energy storage system for high-story buildings. IECEC 96. Proc. 31st Intersoc. Energy Convers. Eng. Conf., vol. 3. 1996. https://doi.org/10.1109/IECEC.1996.553550. p. 2109–14 vol.3.

[11] Guo X, Ma Z, Ma L, Zhang J. Experimental study on the performance of a novel in–house heat pump water heater with freezing latent heat evaporator and assisted by domestic drain water. Appl Energy 2019;235:442–50. https://doi.org/10.1016/j.apenergy.2018.10.094.

[12] Shin HH, Han C, Heo Y, Lee H, Kim Y. Optimal partial-load operation strategies of surface water-source centrifugal heat pumps with thermal energy storage for large buildings. Appl Energy 2025;388:125724. https://doi.org/10.1016/j.apenergy.2025.125724.

[13] Huo D, Wei W, Le Blond S. Optimisation for interconnected energy hub system with combined ground source heat pump and borehole thermal storage 2018;12:529–39.

[14] Naranjo-Mendoza C, Oyinlola MA, Wright AJ, Greenough RM. Experimental study of a domestic solar-assisted ground source heat pump with seasonal underground thermal energy storage through shallow boreholes. Appl Therm Eng 2019;162:114218. https://doi.org/10.1016/j.applthermaleng.2019.114218.

[15] Fiorentini Vivian. Heer, Baldini. Design and optimal integration of seasonal borehole thermal energy storage in district heating and cooling networks. 2022.

[16] Naldi C, Zanchini E. Effects of the total borehole length and of the heat pump inverter on the performance of a ground-coupled heat pump system. Appl Therm Eng 2018;128:306–19. https://doi.org/10.1016/j.applthermaleng.2017.09.025.

[17] Zhu C, Quan C, Shi P, Li B, Zhang J, Li M. Analysis and optimization of a medium-depth ground source heat pump heating systems with heat storage and borehole heat exchangers. Energy Rep 2024;11:1455–71. https://doi.org/10.1016/j.egyr.2024.01.022.

[18] Zhao X, Li Y, Chen X, Yin Y. Ten differences of seasonal borehole thermal energy storage system from ground-source heat pump system. Energ Buildings 2024;325:114994. https://doi.org/10.1016/j.enbuild.2024.114994.

[19] Xue T, Jokisalo J, Kosonen R. Cost-effective control of hybrid ground source heat pump (GSHP) system coupled with district heating. Buildings 2024:14. https://doi.org/10.3390/buildings14061724.

[20] Li X, Yilmaz S, Patel MK, Chambers J. Techno-economic analysis of fifth-generation district heating and cooling combined with seasonal borehole thermal energy storage. Energy 2023;285:129382. https://doi.org/10.1016/j.energy.2023.129382.

[21] Wang Z, Zhou X, Wang F, Sha X, Lu M, Ma Z. Adaptive model-based optimal control of hybrid deep borehole ground source heat pump systems with integrated latent heat thermal energy storage. Appl Energy 2025;390:125737. https://doi.org/10.1016/j.apenergy.2025.125737.

[22] Law YLE, Dworkin SB. Characterization of the effects of borehole configuration and interference with long term ground temperature modelling of ground source heat pumps. Appl Energy 2016;179:1032–47. https://doi.org/10.1016/j.apenergy.2016.07.048.

[23] Yang H, Cui P, Fang Z. Vertical-borehole ground-coupled heat pumps: a review of models and systems. Appl Energy 2010;87:16–27. https://doi.org/10.1016/j.apenergy.2009.04.038.

[24] Zhou Z, Wu S, Du T, Chen G, Zhang Z, Zuo J, et al. The energy-saving effects of ground-coupled heat pump system integrated with borehole free cooling: a study in China. Appl Energy 2016;182:9–19. https://doi.org/10.1016/j.apenergy.2016.07.124.

[25] Hemmatabady H, Formhals J, Welsch B, Schulte DO, Sass I. Optimized layouts of borehole thermal energy storage systems in 4th generation grids. Energies 2020:13. https://doi.org/10.3390/en13174405.

[26] Fiorentini M, Baldini L. Control-oriented modelling and operational optimization of a borehole thermal energy storage. Appl Therm Eng 2021;199:117518. https://doi.org/10.1016/j.applthermaleng.2021.117518.

[27] Arghand T, Javed S, Dalenbäck J-O. Combining direct ground cooling with ground-source heat pumps and district heating: energy and economic analysis. Energy 2023;270:126944. https://doi.org/10.1016/j.energy.2023.126944.

[28] Weeratunge H, Dunstall S, De Hoog J, Narsilio G, Halgamuge S. Optimizing the Operation of a Hybrid Solar Assisted Ground Source Heat Pump System. 2018 IEEE 9th Int Conf Inf Autom Sustain ICIAfS 2018 2018:1–5. doi:https://doi.org/10.1109/ICIAFS.2018.8913385.

[29] Wang JL, Yan T, Tang X, Pan WG. Design and operation of hybrid ground source heat pump systems: a review. Energy 2025;316:134537. https://doi.org/10.1016/j.energy.2025.134537.

[30] Puttige AR, Andersson S, Östin R, Olofsson T. Modeling and optimization of hybrid ground source heat pump with district heating and cooling. Energ Buildings 2022;264:112065. https://doi.org/10.1016/j.enbuild.2022.112065.

[31] Juvelen, Uppsala 2019, https://www.skanska.se/vart-erbjudande/vara-projekt/57898/Juvelen%2C-Uppsala (accessed March 1, 2025).

[32] It's rock science: Drilling deep for low-energy cooling | Skanska - Global corporate website 2023, https://group.skanska.com/media/articles/it-s-rock-science-drilling-deep-for-low-energy-cooling/ (accessed December 14, 2023).

[33] The Köppen Climate Classification 2025, https://www.mindat.org/climate.php (accessed March 28, 2025).

[34] Väder i Uppsala 2023, https://www.smhi.se/q/Uppsala/2666199 (accessed December 14, 2023).

[35] Behzadi A, Holmberg S, Duwig C, Haghighat F, Ooka R, Sadrizadeh S. Smart design and control of thermal energy storage in low-temperature heating and high-temperature cooling systems: a comprehensive review. Renew Sustain Energy Rev 2022;166:112625. https://doi.org/10.1016/j.rser.2022.112625.

[36] Sojoudi M, Li B, Norouzi E. Thermal-hydro-mechanical modeling of short-term ground responses due to the borehole thermal energy storage operations in a Canadian subarctic region. Renew Energy 2024;229:120753. https://doi.org/10.1016/j.renene.2024.120753.

[37] Yang X, Sun D, Li J, Yu C, Deng Y, Yu B. Demonstration study on ground source heat pump heating system with solar thermal energy storage for greenhouse heating. J Energy Storage 2022;54:105298. https://doi.org/10.1016/j.est.2022.105298.

[38] Electricity Maps | Live 24/7 CO_2 emissions of electricity consumption 2025, https://app.electricitymaps.com/map (accessed January 4, 2025).

[39] Spot prices for electricity for the SE3 area - Stockholm | Elbruk.se 2023. https://www.elbruk.se/timpriser-se3-stockholm (accessed December 18, 2025).

[40] Calculate your district heating price | waterfall 2023, https://www.vattenfall.se/foretag/fjarrvarme/priser/berakna-ditt-pris/ (accessed December 15, 2023).

[41] Behzadi A, Sadrizadeh S. Advanced smart HVAC system utilizing borehole thermal energy storage: detailed analysis of a Uppsala case study focused on the deep green cooling innovation. J Energy Storage 2024;99:113470. https://doi.org/10.1016/j.est.2024.113470.

[42] Behzadi A, Duwig C, Ploskic A, Holmberg S, Sadrizadeh S. Application to novel smart techniques for decarbonization of commercial building heating and cooling through optimal energy management. Appl Energy 2024;376:124224. https://doi.org/10.1016/j.apenergy.2024.124224.

[43] Up W. Ground source heat pump this is how F1345 works. https://www.nibe.eu/en-eu/products/heat-pumps; 2025 (accessed March 1, 2025).